# UNITED TECHNOLOGIES RESEARCH CENTER

East Hartford, Connecticut 06108



NASA CR-159430


# DERIVATION AND EVALUATION OF AN APPROXIMATE ANALYSIS FOR THREE-DIMENSIONAL VISCOUS SUBSONIC FLOW WITH LARGE SECONDARY VELOCITIES


by Olof L. Anderson

APPENDIX BY

W. R. Briley and H. McDonald



Prepared under Contract No. NAS3-19752 by
UNITED TECHNOLOGIES RESEARCH CENTER
East Hartford, Connecticut

for

NATIONAL AERONAUTICS AND SPACE ADMINISTRATION




UNITED TECHNOLOGIES

**UNITED TECHNOLOGIES RESEARCH CENTER**

East Hartford, Connecticut 06108

October 24, 1978

NASA Scientific and Technical Information Facility
P. O. Box 8757
Balt/Wash International Airport
Maryland 21240

Attention: Accessioning Department

Subject: Final Report for NASA Contract NAS3-19752
"Derivation and Evaluation of an Approximate Analysis for Three-Dimensional Viscous Subsonic Flow with Large Secondary Velocities"

Gentlemen:

Enclosed are thirty (30) copies of the corrected subject report.

The Document Release Authorization form was forwarded to you on October 12. If another form is needed, please forward it to us and we will fill it out and return it to you.

Sincerely,

MJWerle

M. J. Werle
Chief, Gas Dynamics Section

MJW:jm
Enclosures

| 1 Report No | 2 Government Accession No | 3 Recipient's Catalog No |
|---|---|---|
| NASA CR-159430 | | |

| 4 Title and Subtitle | 5 Report Date |
|---|---|
| Derivation and Evaluation of an Approximate Analysis for Three-Dimensional Viscous Subsonic Flow With Large Secondary Velocities | October 1978 |
| | 6 Performing Organization Code |

| 7 Author(s) | 8 Performing Organization Report No |
|---|---|
| O. L. Anderson<br>W. R. Briley<br>H. McDonald | UTRC78-106 |
| | 10 Work Unit No<br>YON 6645 |

| 9 Performing Organization Name and Address | 11 Contract or Grant No |
|---|---|
| United Technologies Research Center<br>East Hartford, Connecticut 06108 | NAS3-19752 |
| | 13 Type of Report and Period Covered<br>Contractor Report |

| 12 Sponsoring Agency Name and Address | 14 Sponsoring Agency Code |
|---|---|
| National Aeronautics and Space Administration<br>Lewis Research Center<br>Cleveland, Ohio 44135 | |

15 Supplementary Notes

Project Manager: E. R. McFarland
National Aeronautics and Space Administration
Lewis Research Center, Cleveland, Ohio 44135

16 Abstract

An approximate analysis is presented for calculating three-dimensional, low Mach number, laminar viscous flows in curved passages with large secondary flows and corner boundary layers. The analysis is based on the decomposition of the overall velocity field into "inviscid" and "viscous" components with the overall velocity being determined from superposition. An incompressible vorticity transport equation is used to estimate inviscid secondary flow velocities to be used as corrections to the potential flow velocity field. A "parabolized" streamwise momentum equation coupled to an adiabatic energy equation and global continuity equation is used to obtain an approximate viscous correction to the pressure and longitudinal velocity fields. A collateral flow assumption is invoked to estimate the viscous correction to the transverse velocity fields. The approximate analysis is solved numerically using an implicit ADI solution for the "viscous" pressure and velocity fields and an iterative ADI procedure is used to solve for the inviscid secondary vorticity and velocity fields.

This method was applied to computing the flow within (a) a turbine vane passage with inlet flow conditions of M = 0.1 and M = 0.25, Re = 1000 and adiabatic walls, and (b) a constant radius curved rectangular duct with R/D = 12 and 14 and with inlet flow conditions of M = 0.1, Re = 1000, and adiabatic walls. In the latter case a comparison is made with experimental data.

A description of the operation and details of the computer code is also presented.

| 17 Key Words (Suggested by Author(s)) | 18 Distribution Statement |
|---|---|
| Propulsion<br>Three Dimensional<br>Finite Difference Solution | Unclassified<br>Publically Available |

| 19 Security Classif (of this report) | 20 Security Classif (of this page) | 21 No of Pages | 22 Price* |
|---|---|---|---|
| Unclassified | Unclassified | 82 | |

* For sale by the National Technical Information Service, Springfield Virginia 22161

# Derivation and Evaluation of an Approximate Analysis For Three-Dimensional Viscous Subsonic Flows with Large Secondary Velocities

TABLE OF CONTENTS


| | | Page |
|---|---|---|
| FOREWORD | | i |
| 1.0 | SUMMARY | 1-1 |
| 2.0 | INTRODUCTION | 2-1 |
| 3.0 | ANALYSIS | 3-1 |
| | 3.1 Basic Concept | 3-1 |
| | 3.2 Governing Equations | 3-2 |
| | 3.3 Numerical Analysis | 3-5 |
| 4.0 | CALCULATION RESULTS | 4-1 |
| | 4.1 Turbine Vane Passage | 4-1 |
| | 4.2 Circular Arc Duct | 4-5 |
| 5.0 | CONCLUSIONS | 5-1 |
| 6.0 | REFERENCES | 6-1 |
| 7.0 | LIST OF SYMBOLS | 7-1 |
| 8.0 | FIGURES AND TABLES | 8-1 |
| 9.0 | PROGRAM DESCRIPTION | 9-1 |
| 10.0 | APPENDICES | 10-1 |
| 11.0 | DETAILED PROGRAM DESCRIPTION | 11-1 |

# FOREWORD

The analysis and development of the computer code described herein were initiated by W. R. Briley and H. McDonald while at the United Technologies Research Center, and completed by Briley and McDonald at the Scientific Research Associates Inc. under subcontract to United Technologies Research Center. In addition SRA Inc. provided consulting assistance in the description of the computer code interfacing given in Section 9.7 and in its application to the test case described in Section 4.2. The details of the computing procedure with additional results obtained by SRA are given in Section 10.0 together with the complete Sub-Contractor's report.

# 1.0 SUMMARY

An approximate analysis is presented for calculating three-dimensional, low Mach number, laminar viscous flows in curved passages with large secondary flows and corner boundary layers. The analysis is based on the decomposition of the overall velocity field into "inviscid" and "viscous" components with the overall velocity being determined from superposition. An incompressible vorticity transport equation is used to estimate inviscid secondary flow velocities to be used as corrections to the potential flow velocity field. A "parabolized" streamwise momentum equation coupled to an adiabatic energy equation and global continuity equation is used to obtain an approximate viscous correction to the pressure and longitudinal velocity fields. A collateral flow assumption is invoked to estimate the viscous correction to the transverse velocity fields. The approximate analysis is solved numerically using an implicit ADI solution for the "viscous" pressure and velocity fields and an iterative ADI procedure is used to solve for the inviscid secondary vorticity and velocity fields.

This method was applied to computing the flow within (a) a turbine vane passage with inlet flow conditions of $M = 0.1$ and $M = 0.25$, $Re = 1000$ and adiabatic walls, and (b) a constant radius curved rectangular duct with $R/D = 12$ and 14 and with inlet flow conditions of $M = 0.1$, $Re = 1000$, and adiabatic walls. In the latter case a comparison is made with experimental data.

A description of the operation and details of the computer code is also presented.

## 2.0 INTRODUCTION

Future gas turbine engines will employ higher turbine inlet temperatures to achieve higher cycle efficiencies. An important consideration in the design of gas turbine engines therefore is the accurate prediction of loss and heat transfer in the region of the turbine end wall where large secondary flows and corner boundary layers occur. The flow in this region is three-dimensional and can not be treated by an inviscid-viscous boundary layer interaction approach. Although direct numerical solution of the Navier-Stokes equations is possible, it is costly and time consuming on the computer. Therefore, efforts have been made to simplify the governing equations by neglecting streamwise diffusion and thus reduce the Navier-Stokes equations, which are elliptic, to a parabolic set of equations which can be integrated by forward marching numerical methods.

Efforts to integrate these parabolic equations have been successful for straight ducts of rectangular cross section (Refs. 1, 2, 3). Even these methods, however, require further simplification of the problem by splitting the pressure into viscous and inviscid terms and treating the transverse momentum equations differently from the streamwise momentum equation. This method has been extended to ducts with other cross sections (Ref. 4) and to circular arc ducts of rectangular cross section with a large radius of curvature (Ref. 5). For all of these problems the secondary flow was small.

In the turbine end wall problem the flow curvature and secondary flows are much larger and strong "elliptic" effects are present. Therefore it is to be anticipated that methods developed for flows with small curvature will encounter difficulty in these cases mainly due to the manner in which the local pressure distribution and transverse momentum laws are approximated. The purpose of this study is first to develop an approximate forward marching analysis for flows in ducts with large curvature and secondary flows and secondly, through numerical experimentation, to assess the analytic model and its capability for predicting end-wall losses and heat transfer in a vane passage.

# 3.0 ANALYSIS

## 3.1 Basic Concepts

A cross section of a simulated turbine vane passage duct geometry is shown in Fig. 1 and consists of two curved walls corresponding to the surfaces of the turbine airfoils. The remaining boundaries of the flow passage are two parallel flat surfaces comprising the endwalls. The geometry and inviscid flow, therefore, are two-dimensional. However, the viscous flow is three-dimensional, particularly near the endwalls, where the transverse pressure gradients associated with the turning of the flow produce strong secondary flow toward the low pressure or suction surface side of the passage.

Coordinate System

Curvilinear orthogonal coordinates x, y, z are constructed to fit the flow passage boundaries as shown in Fig. 1. Metric coefficients $h_1$, $h_2$, $h_3$ are defined such that incremental distance $\delta s$ is determined by $(\delta s)^2 = (h_1 \delta x)^2 + (h_2 \delta y)^2 + (h_3 \delta z)^2$. In the planes parallel to the endwalls, orthogonal streamlines and velocity potential lines from a two-dimensional incompressible potential flow analysis are utilized as the coordinate lines for constant y and x, respectively. The z direction can be regarded as Cartesian, and thus $h_3 = 1$. The x coordinate is the primary flow or axial coordinate, and is associated with surfaces for which $\phi_I$ is constant. The y and z coordinates define transverse secondary flow planes at any given x location. In this coordinate system, the potential flow direction $\bar{i}_p$ and the normals $\bar{i}_n$ to the transverse planes coincide with $\bar{i}$, the unit vector in the x direction. A two-dimensional incompressible potential flow analysis and computer program developed by Anderson (Ref. 6) was employed in the present investigation, without modification, to compute the necessary coordinate data and potential flow solution.

## 3.2 Governing Equations

The complete derivation of the governing equation for the approximate flow field description employed in this study are presented in Section 10.0, Appendix A, of this report. The resulting equations as they apply to the present geometry are presented in detail in the following discussion.

All variables used in the following governing equations are nondimensional having been normalized by the following reference quantities: distance, $L_r$; velocity, $U_r$; density, $\rho_r$; temperature, $T_r$; total enthalpy, $U_r^2$; pressure, $\rho_r U_r^2$ viscosity, $\mu_r$. These quantities may be specified arbitrarily. This normalization leads to the following nondimensional parameters: Mach number, M; Reynolds

number, Re; Prandtl number, Pr; and specific heat ratio, $\gamma$. These parameters are defined by

$$M = U_r/c \ , \ Re = \rho_r U_r L_r/\mu_r \ , \ Pr = c_p \mu_r / k \ , \ \gamma = c_p / c_v \qquad (3.1)$$

where $\mu_r$ is the molecular viscosity, k is thermal conductivity, and $c_p$ and $c_v$ are the specific heats at constant pressure and volume. The reference speed of sound, c, is defined by $c^2 = \gamma R_g T_r$, where $R_g$ is the gas constant.

Since in the present application the coordinate lines coincide with the potential flow streamlines and potential surfaces, the following simplifications hold: $v_I = w_I = u_s = 0$. The velocity decomposition Eq. (10.3.2) can thus be expressed as

$$\bar{U} = \bar{i}u + \bar{j}v + \bar{k}w = \bar{i}(u_I + u_v) + \bar{j}(v_s + v_v) + \bar{k}(w_s + w_v) \qquad (3.2)$$

where $\bar{i}$, $\bar{j}$, $\bar{k}$ are unit vectors in the x, y, z coordinate directions, respectively. The incompressible streamwise vorticity equation, Eq. (10.2.6) can be written

$$\frac{u_I}{Q}\left(u\frac{\partial \xi}{\partial x} - \xi\frac{\partial u}{\partial x}\right) + \frac{v_s}{Q}\frac{h_1}{h_2}\left(u\frac{\partial \xi}{\partial y} - \xi\frac{\partial u}{\partial y}\right) + \frac{w_s}{Q}h_1\left(u\frac{\partial \xi}{\partial z} - \xi\frac{\partial u}{\partial z}\right)$$

$$= -\frac{2}{h_2}\frac{\partial h_1}{\partial y}u\frac{\partial u}{\partial z} + \frac{\mu}{Re}\left(\frac{\partial}{\partial y}\frac{1}{h_1 h_2}\frac{\partial h_1 \xi}{\partial y} + h_1\frac{\partial^2 \xi}{\partial z^2}\right) \qquad (3.3a)$$

This vorticity transport equation, Eq. (3.3a), is derived in Section 10.0 with the following assumptions:

1) the flow is incompressible;

2) streamwise diffusion is negligible;

3) the secondary vorticity vector lies in the direction of primary potential flow (i.e., coordinate direction through the same channel geometry;

4) the principal streamline curvature is obtained from a primary potential flow solution;

and is solved with the boundary condition $\xi = 0$ on the wall. It should be noted that Eq. (3.3a) is an approximate representation of the full vorticity equation and as such is limited in its ability to properly model vorticity near the wall for two specific reasons. First, in the exact equation, Eq. (10.2.6), the convection velocities vanish at the wall, whereas in Eq. (3.3a) convection does not. Secondly, since vorticity can be generated only at a no slip surface, the boundary condition $\xi = 0$ may not adequately model the generation of new vorticity at the wall.

In equation (3.3a) $Q^2 = u_I^2 + v_s^2 + w_s^2$, and the vorticity is related to velocity by

$$\xi_n = \xi = \frac{1}{h_2}\left(\frac{\partial w_s}{\partial y} - \frac{\partial h_2 v_s}{\partial z}\right) \tag{3.3b}$$

The secondary velocities are given by

$$v_s = \frac{1}{h_2}\frac{\partial \phi_s}{\partial y} + \frac{1}{h_1}\frac{\partial h_1 \psi_s}{\partial z} \tag{3.4a}$$

$$w_s = \frac{\partial \phi_s}{\partial z} - \frac{1}{h_1 h_2}\frac{\partial h_1 \psi_s}{\partial y} \tag{3.4b}$$

where the scalar and vector potential functions $\phi_s$ and $\psi_s$ are governed by

$$\frac{1}{h_2}\frac{\partial}{\partial y}\frac{1}{h_1 h_2}\frac{\partial}{\partial y} h_1 \psi_s + \frac{1}{h_1}\frac{\partial^2 h_1 \psi_s}{\partial z^2} = -\xi \tag{3.5}$$

and

$$\frac{\partial}{\partial y}\frac{h_1}{h_2}\frac{\partial \phi_s}{\partial y} + h_1 h_2 \frac{\partial^2 \phi_s}{\partial z^2} = -\left(\frac{\partial h_2 u_v}{\partial x} + \frac{\partial h_1 v_v}{\partial y} + \frac{\partial h_1 h_2 w_v}{\partial z}\right) \tag{3.6}$$

Eq. 3.5 and 3.6 assume incompressible flow and are solved with slip boundary conditions. The streamwise momentum equation, Eq. (10.2.15), is approximated by

$$\begin{aligned} &\frac{\partial}{\partial x}(h_2 \rho u^2) + \left[\frac{\partial}{\partial y} + \frac{1}{h_1}\frac{\partial h_1}{\partial y}\right] h_1 \rho u (v_s + v_v) + h_1 h_2 \frac{\partial}{\partial z}\left[\rho u (w_s + w_v)\right] \\ &- \rho (v_s + v_v)^2 \frac{\partial h_2}{\partial x} + h_2 \frac{\partial (p_I + p_s)}{\partial x} + h_2 \frac{dp_v(x)}{dx} \\ &= \frac{\hbar}{Re}\frac{\partial}{\partial y}\frac{\mu}{h_2}\frac{\partial u}{\partial y} + \frac{h_1 h_2}{Re}\frac{\partial}{\partial z}\mu\frac{\partial u}{\partial z} \end{aligned} \tag{3.7}$$

Eq. (3.7) is solved with no slip boundary conditions and is derived in Section 10.0 with the following assumption:

1) Streamwise diffusion is negligible;

2) the pressure can be split into viscous and inviscid terms in which the viscous term, $p_v$, is a function of only the longitudinal coordinate, x.

An important result of this approximation is that transverse pressure gradients are set entirely by the calculated inviscid flow field $p_I$ and $p_s$.

The energy equation, Eq. (10.2.23) is approximated by

$$\frac{\partial}{\partial x}(h_2\rho uE) + \frac{\partial}{\partial y}\left[h_1\rho(v_s+v_v)E\right] + \frac{\partial}{\partial z}\left[h_1h_2\rho(w_s+w_v)E\right]$$
$$= \frac{h_1}{Re}\frac{\partial}{\partial y}\left\{\frac{\mu}{Pr}\frac{1}{h_2}\frac{\partial E}{\partial y} + \frac{1}{2h_2}\left(\mu-\frac{\mu}{Pr}\right)\frac{\partial}{\partial y}\left[u^2+(w_s+w_v)^2\right]\right\} \qquad (3.8)$$
$$+ \frac{h_1h_2}{Re}\frac{\partial}{\partial z}\left\{\frac{\mu}{Pr}\frac{\partial E}{\partial z} + \frac{1}{2}\left(\mu-\frac{\mu}{Pr}\right)\frac{\partial}{\partial z}\left[u^2+(v_s+v_v)^2\right]\right\}$$

Eq. (3.8) neglects streamwise diffusion of heat (heat conduction). It should be noted that a number of previous equations, namely Eq. (3.3) through Eq. (3.6), were derived for incompressible flow and therefore calculated results for temperature should be examined closely if compressibility effects are significant.

The imposed pressure gradients are determined from an inviscid streamwise momentum equation, Eq. (10.2.18) given as

$$h_2\frac{\partial(p_I+p_s)}{\partial x} = -\frac{\partial}{\partial x}(h_2u_I^2) - \left[\frac{\partial}{\partial y} + \frac{1}{h_1}\frac{\partial h_1}{\partial y}\right]h_1u_Iv_s - h_1h_2\frac{\partial}{\partial z}u_Iw_s + v_s^2\frac{\partial h_2}{\partial x} \qquad (3.9)$$

Eq. (3.9) is essentially the Euler equation for the primary potential and inviscid secondary flows and is related to the dependent variables using the following form of the auxiliary gas law relation, Eq. (10.2.25)

$$\frac{\partial}{\partial x}\left[\frac{\gamma-1}{\gamma}\rho\left(E-\frac{u^2}{2}\right)\right] = \frac{\partial(p_I+p_s)}{\partial x} + \frac{dp_v(x)}{dx} \qquad (3.10)$$

The integral mass flux relation is

$$\iint_A h_2\rho u\,dydz = \text{constant} \qquad (3.11)$$

To obtain the viscous contributions to the transverse velocity field, the momentum conservation law is dropped in favor of algebraic relations obtained from assuming that the flow is collateral (see Eq. (10.2.22), leading to the following equations for computing $v_v$, $w_v$:

$$v_v = v_s\left(\frac{u}{u_I} - 1\right) \qquad (3.12a)$$

$$w_v = w_s\left(\frac{u}{u_I} - 1\right) \qquad (3.12b)$$

### 3.3 Numerical Analysis

The governing equations are replaced by finite-difference approximations. Three-point central difference formulas are used for all transverse spatial derivatives. An analytical coordinate transformation devised by Roberts (Ref. 7) is employed as a means of introducing a nonuniform grid in each transverse coordinate direction, to concentrate grid points in the wall boundary layer regions. Second-order accuracy for the transverse directions is rigorously maintained. Two-point backward difference approximations are used for streamwise derivatives. The streamwise vorticity equation (3.3) is decoupled from other equations in the system and linearized with respect to $\xi$ by an ad hoc process consisting of lagging quantities not yet available at the implicit level. The resulting implicit difference equation for $\xi$ is solved using a scalar ADI scheme based on the technique of Douglas & Gunn (Ref. 8) for generating ADI schemes as perturbations of fundamental implicit schemes. Equations (3.5 - 3.6) for the scalar and vector potential functions $\phi_s$ and $\psi_s$ are elliptic in the transverse planes and are solved, given values for the right-hand sides, using scalar iterative ADI. Specifically, the Douglas-Gunn perturbation of the Crank-Nicolson scheme is used. The streamwise momentum (3.7), energy (3.8) and auxiliary gas law relation (3.10) are solved as a coupled system using linearized block ADI. A detailed discussion of the block ADI scheme used has been given by McDonald & Briley (Ref. 9) and Briley & McDonald (Ref. 10). The general approach is to linearize the implicit equations by formal expansion about the solution at the most recent axial location. Terms in the difference equations are then grouped by coordinate direction, and the Douglas-Gunn (Ref. 8) technique is used to generate an ADI scheme. The resulting difference equations can be written in block-tridiagonal or a closely related matrix form and solved efficiently by block elimination techniques.

A summary of the overall algorithm used to advance the solution a single axial step follows. It is assumed that the solution is known at the n level $x^n$ and is desired at $x^{n+1}$.

1. The streamwise vorticity equation (3.3) is solved using scalar ADI to obtain $\xi^{n+1}$.

2. The vector potential equation (3.5) is solved using scalar iterative ADI to obtain $\psi_s^{n+1}$.

3. Values for $v_s$ and $w_s$ are computed using equation (3.4). Values of $\phi_s^n$ obtained from the previous step are used. Values for $v_v$ and $w_v$ are computed from equations (3.12). The imposed pressure gradients $\partial(p_I + p_s)/\partial x$ are computed from equation (3.9).

4. A value for the mean viscous pressure drop $dp_v(x)/dx$ is assumed. Initally, the value from the previous step is used.

5. Equations (3.7), (3.8), & (3.10) are solved as a coupled system using block ADI to obtain values of $u^{n+1}$, $\rho^{n+1}$ and $E^{n+1}$. In general, the integral mass flux relation (3.11) will not be satisfied.

6. Step 4 is repeated and this process is continued iteratively using the standard secant method (Ref. 11) to find the value of the mean viscous pressure drop which leads to $u^{n+1}$ and $\rho^{n+1}$ and satisfies the integral mass flux relation Eq. (3.11). The secant method was found in practice to converge to five figures on the third iteration.

7. Using values now available for $\partial u/\partial x$, the scalar potential equation (3.6) is solved using scalar iterative ADI to obtain $\phi_s^{n+1}$ for use in the next axial step.

To start this procedure, values for $\phi^n$ are needed. These are obtained by solving steps (4-7) above, under the assumption that the transverse velocity components are known and for these cases taken to be zero.

# 4.0 CALCULATION RESULTS

The analysis for the flow field in a turbine vane passage in Section 3 must be considered approximate. A number of assumptions have been made including: (1) neglect of streamwise diffusion in the equations of motion, (2) decomposition of the velocity and pressure fields into viscous and inviscid terms, (3) use of an incompressible vorticity transport equation with inviscid velocities to estimate the secondary vorticity, (4) a "viscous" static pressure field which varies only in the marching direction, (5) algebraic approximations to the "viscous" transverse velocity field. Several test cases are presented here to assist in assessing the range of applicability and utility of the approximate model used to determine the flow field properties.

The first case is laminar flow through a simulated turbine vane passage; the second case is laminar flow through the same turbine vane passage with a higher inlet dynamic pressure. Finally, two cases are presented for laminar flow through a circular arc duct for which experimental data are available.

## 4.1 Turbine Vane Passage

The geometry of the simulated turbine vane passage is shown in Fig. 1. Upstream and downstream of the blades, the duct walls are assumed tangent to the inlet and exit velocities. The effect of the blade leading edge and trailing edge are neglected. Since the turbine geometric parameters such as twist, pitch, and chord are constant in the spanwise direction, the inviscid flow field is quasi two dimensional and can be constructed from the plane potential flow solution. This plain potential flow is shown on Fig. 1 and is used to construct an orthogonal coordinate system according to the method of Ref. [6] in which the stream function and velocity potential become the normal and streamwise coordinate. These streamlines define the primary flow direction and the direction of the streamwise vorticity.

### Small Inlet Dynamic Pressure

A laminar flow calculation was performed on a 20 x 20 grid with 24 full streamwise steps or 48 ADI half steps. The initial conditions were for an inlet Mach number, M, = .1 and a Reynolds number, Re, = 1000. The remaining parameters for this test case are shown on Table I. As can be seen from Table I, the viscosity was adjusted to fix Reynolds numbers and Mach numbers and hence does not represent a value for air at these conditions. The run time for this case on a UNIVAC 1110 was 40 minutes. This run time was found to vary somewhat from case to case depending on the rate of convergence of the internal ADI iteration process.

The calculated streamwise vorticity distribution at the last two stations is shown on Fig. 2. This vorticity is the component aligned in the primary flow direction and produces the secondary flow velocities which lie in planes normal to the primary flow as defined in Refs. 12, 13. A large region of vorticity is apparent

on the suction side of the turbine endwall passage which may be identified as vortex roll up. The computational grid used in obtaining this result is superimposed on the solution at the last station. Grid points close to the wall are not shown because they are too dense to plot. These results appear qualitively reasonable within present knowledge of the flow field.

The quantitative distribution of secondary vorticity is shown in Fig. 3. Again the abscissa is the distance across the gap and several slices are shown at increasing distance from the end wall out to the plane of symmetry. Note that the axis has been shifted vertically to assist in interpretation of results. In general it is seen that regions of vorticity occur near the suction side of the duct passage consistant with the vortex roll up process observed in Fig. 2. However, it is observed that the vorticity distribution is very irregular and in some cases two extrema appear with an intermediate reversal in sign for some cases. It would appear that the rather rapid decreases in vorticity, $\xi$, near the walls and subsequent rapid increase across the gap is a direct result of the use of the inviscid boundary condition of zero vorticity on the walls - thereby raising some concern about the quantitative reliability of the approximate model being used to determine the local flow field properties.

The gapwise and spanwise secondary flow velocities obtained using this vorticity field are shown on Figs. 4 and 5, respectively. The secondary flow is seen to move across the gap from the pressure to suction side, then spanwise along the suction surface, back across the gap near the mid plane and finally down along the pressure surface. The grid points are shown as data points indicating sufficient resolution. Such a secondary flow field does not appear to be consistant with the secondary flow analysis developed in Refs. 12 and 13.

The streamwise velocity distribution of the primary flow for this case is shown on Fig. 6. The abscissa is the distance across the gap, and several slices are shown at increasing distance from the end wall out to the plane of symmetry. These velocity distributions indicate that relatively thin boundary layers exist throughout the flow field despite the rather low Reynolds number of 1000. Also note should be taken of a small local extrema in the velocity distribution in the suction corner which may be caused by the large secondary vorticity. However, it should be noted that the viscous transverse velocities are not obtained by integrating the vorticity equation Eq. (3.3b) but rather by using an algebraic relation Eq.(3.12). In effect, the two transverse momentum equations have been replaced by two approximate algebraic relations. Since the transverse momentum equation relates pressure gradient, acceleration, and diffusion of vorticity; care should be taken in constructing this approximate model to show that the transverse momentum equations are satisfied.

In an attempt to assess the internal consistency of the approximate model being used here, attention was given to its ability to predict the total pressure loss through the passage region. Since no external work is done on the flow, only viscous work, no streamline should leave the duct with a total pressure larger than the maximum inlet total pressure. Thus a total pressure loss coefficient referenced

to the maximum inlet total pressure must always be greater than zero. This calculation for the exit flow in the present case is shown in Fig. 7. Significant regions of total pressure greater than the maximum inlet total pressure are shown as the crosshatched region with the worse case occurring near the hub. The large increase in total pressure is apparently due to the pressure decomposition and approximation procedures used in the present approach. Since the dynamic head was very small for the current test case (and thus the dynamic pressure q was quite small) it is also clear that the numerical truncation errors of the current approach could be contributing to this anomalous behavior. A subsequent calculation of higher Mach number (and thus higher $q_r$) will be discussed later to give more insight into this problem.

A final consistency argument can be made with regard to the transverse pressure gradients obtained from the current approximate analysis. Since the two transverse momentum equations are not used in the analysis; they may be used as "a postori" tests of the accuracy of the solution. On the endwall, the transverse momentum equation reduces to

$$\frac{1}{h_2}\frac{\partial P}{\partial y_2} = \frac{\mu}{h_3}\frac{\partial \xi}{\partial y_3} \tag{4.1}$$

thus relating transverse pressure gradient to vorticity gradient. Eq. (4.1) has been integrated along the endwall using the value of $\xi$ from the solution of equation (3.3a). The resulting pressure distribution is compared with that obtained from the present approximate model, Eq. (10.2.16), in Figure 8. Clearly the transverse pressure field obtained from Eq. (10.2.16) is not in balance with the transverse momentum equation and additional work may be required on this approximate model of the flow field.

Large Inlet Dynamic Pressure

The baseline test case study for laminar flow through the turbine duct presented above was performed for an inlet Mach number M = .1. Therefore the dynamic pressure at the inlet was less than one percent of the static pressure so that small errors in calculating static pressure could lead directly to significant errors in the static pressure and total pressure coefficient. Therefore in order to assess the level of accuracy being achieved in predicting pressure levels, the baseline test case was rerun with a higher inlet Mach number (M = 0.25) to produce an inlet dynamic pressure 7 times that of the base case (Case 2 Table I). The calculated results for total pressure loss distribution are shown on Fig. 9. Again regions of significant gain are encountered with only marginal improvement over the lower Mach number results. It is apparent that the total pressure loss through the duct is not yet adequately represented by this approximate flow field model.

A final note should be made concerning this case. Since the vorticity transport equation (3.3) is incompressible and the complete energy equation is not used

(Eq. 3.12), the calculation is more nearly an incompressible flow calculation although density and temperature variations occur. Thus when the inlet Mach number $M_r$ was raised to .25 and subsequently to .30, the calculation failed half way through the duct at approximately the minimum area ratio. The indicated Mach numbers at this last station were M = .87 for the $M_r$ = .25 case and M = 1.4 for the $M_r$ = .30 case. These observations indicate that calculations at higher Mach numbers where compressibility is significant may not yet be reliable.

## 4.2 Circular Arc Duct

The case of flow in a circular arc duct represents an important problem because for some configurations comparisons can be made with experimental data published by Mori (Ref. 14). The general geometry of this case is shown in Fig. 10 along with the definition of the principal parameters effecting the solution. Of these parameters, the most important is Dean's number which represents the ratio of the viscous force to transverse static pressure force. The flow parameters for these cases, designated 3 and 4 in Table I, represent the flow in a square duct with different step size so that the flow turns through $90^{o}$ and $220^{o}$, rspectively. Of these parameters, it should be noted that $\hat{R}e_d$ is based on hydraulic dyameter and $R_e$ on gap width.

The solution for the developing profile of the streamwise velocity at the plane of symmetry for case 3 is shown on Fig. 11. For this case, as in previous cases, the integration used a 20 x 20 mesh in the transverse plane and 24 streamwise stations for a streamwise steps size $\Delta\theta = 3.68^{o}$. The growth of the wall boundary layer is clearly evident and the free stream shows a pronounced velocity gradient with a peak on the suction side of the duct. This velocity gradient is much larger than would be obtained by simple radial equilibrium of two dimensional flow, thus indicating substantial secondary flow effects.

A second case was run for the circular arc duct (case 4) which was the same as case 3, but with a larger step size $\Delta\theta = 11.05^{o}$. For this case the flow made a turn of $220^{o}$. The streamwise velocity distribution at the plane of symmetry at $220^{o}$ is shown at Fig. 12 where it is compared with the experimental data of Mori (Ref. 14). This comparison is quite good in the mid-stream region and indicates that the essential secondary flow phenomena is well represented by the vorticity transport equation. Considering the assumptions made for the vorticity transport equation (Eq. 3.3), it may be concluded that a large region of the secondary flow in the midspan region is essentially inviscid and can be represented fairly well by Eq. 3.7. Near the wall, however, insufficient data exists to verify the approximate model used in these calculations. In particular, as shown on Fig. 12, a noticable difference exists between the calculated velocity and measured velocity near the pressure side of the duct. This difference may be due to the inviscid boundary conditions on the vorticity transport equation.

# 5.0 CONCLUSIONS

Based on the results presented in this study it can be concluded that:

1. - The explicit use of the vorticity transport equation to describe secondary flows and its interaction with the primary streamwise flow leads to the appearance of a clearly defined passage vortex.

2. Approximations used in the analysis, including pressure splitting and inviscid like boundary conditions on the vorticity transport equation may effect quantitative predictions.

3. Insufficient experimental data exists to verify the approximate flow model in regions of large secondary flow velocities.

In particular, the accuracy of the flow conditions at and near the wall would be expected to be sensitive to the approximations made in constructing and solving the local flow model.

## 6.0 REFERENCES


1. Patankar, S. V. and D. B. Spalding: A Calculation Procedure for Heat, Mass, and Momentum Transfer in Three-Dimensional Parabolic Flows. Int. J. Heat and Mass Transfer, Vol. 15, p. 1787, 1972.

2. Caretto, L. S., R. M. Curr and D. B. Spalding: Two Numerical Methods for Three-Dimensional Boundary Layers. Computational Methods in Applied Mechanics and Engineering, Vol. 1, p. 39, 1973.

3. Briley, W. R.: Numerical Method for Predicting Three-Dimensional Steady Viscous Flow in Ducts. Journal of Computational Physics, Vol. 14, p. 8, 1974.

4. Ghia, K. N., V. Ghia and C. J. Studerus: Analytical Formulation of Three-Dimensional Laminar Viscous Flow Through Turbine Cascade Using Surface-Oriented Coordinates. ASME Paper No. 76-FE-22, 1976.

5. Ghia, K. N. and J. S. Sokhey: Laminar Incompressible Viscous Flow in Curved Ducts of Rectangular Cross-Sections. J. Fluids Engineering, Vol. 99, p. 640, 1977.

6. Anderson. O. L.: User's Manual for a Finite-Difference Calculation of Turbulent Swirling Compressible Flow in Axisymmetric Ducts with Struts and Slot Cooled Walls. USAAMRDL-TR-74-50, Vol. I., 1974.

7. Roberts, G. O.: Computational Meshes for Boundary Layer Problems. Proceedings of the Second International Conference on Numerical Methods in Fluid Dynamics. Springer-Verlag, New York, p. 171, 1971.

8. Douglas, J. and J. E. Gunn: A General Formulation of Alternating Direction Methods, Part I. Parabolic and Hyperbolic Problems. Numerische Mathematik, Vol. 6, p. 428, 1964.

9. McDonald, H. and W. R. Briley: Three-Dimensional Supersonic Flow of a Viscous or Inviscid Gas. Journal of Computational Physics, Vol. 19, No. 2, p. 150, 1975.

10. Briley, W. R. and H. McDonald: Solution of the Multidimensional Compressible Navier-Stokes Equations by a Generalized Implicid Method. J. Comp. Phys., Vol. 24, p. 372, 1977.

11. Ralston, A.: A First Course in Numerical Analysis. McGraw-Hill, New York, p. 323, 1965.

## 6.0 REFERENCES (Con'd)


12. Squire, H. B. and K. G. Winter: The Secondary Flow in a Cascade of Airfoils in a Non-Uniform Stream. J. Aero. Sci., Vol. 18, p. 271, 1951.

13. Hawthorne, W. R.: The Applicability of Secondary Flow Analyses to the Solution of Internal Flow Problems. Fluid Mechanics of Internal Flow, Gino Sovran, Ed., Elsevier Publishing Co., New York, New York, 1967.

14. Mori, Y., Y. Uchida and T. Ukon: Forced Convection Heat Transfer In a Curved Channel of Square Cross Section. Int. J. Heat Mass Transfer, Vol. 14, pp. 1787-1805, 1971.

15. Horlock, J. H. and B. Lakshminarayana: Secondary Flow; Theory, Experiment and Application in Turbomachinery Aerodynamics. Annual Reviews in Fluid Mechanics, Vol. 5, p. 247, 1973.

16. Lakshminarayana, B. and J. H. Horlock: Generalized Expressions for Secondary Vorticity Using Intrinsic Coordinates, J. Fluid Mech., Vol. 59, p. 97, 1973.

17. Stuart, A. R. and R. Hetherington: The Solution of the Three Variable Duct Flow Equations. Fluid Mechanics, Acoustics and Design of Turbomachinery, NASA SP-304, pp. 135-154, 1974.

18. Nash, J. F. and V. C. Patel: Three-Dimensional Turbulent Boundary Layers. SBC Technical Books, Atlanta, 1972.

19. Rubin, S. G. and P. K. Khosla: Laminar Flow in Rectangular Channels, Part II - Numerical Solution for a Square Channel. Computer Methods in Fluid Mechanics, ASME, p. 29, 1976.

20. Patankar, S. V., V. S. Pratap and D. B. Spalding: Prediction of Laminar Flow and Heat Transfer in Helically Coiled Pipes. Journal of Fluid Mechanics, Vol. 62, p. 539, 1974.

21. Newell, A. E.: Vector Analysis. McGraw-Hill, New York, p. 116, 1955.

22. Johnston, J. P.: On the Three-Dimensional Turbulent Boundary Layer Generated by Secondary Flow. J. Basic Engineering, Vol. 82, p. 233, 1960.

# 7.0 LIST OF SYMBOLS

| | |
|---|---|
| $C$ | Speed of Sound |
| $C_p$, $C_u$ | Specific Heats |
| $C_p$ | Pressure Coefficient |
| $D$ | Hydraulic Dynameter |
| $E$ | Internal Energy $C_pT$ |
| $G$ | Gap |
| $h_1, h_2, h_3$ | Metni Scale Coefficients |
| $K$ | Dean's Number |
| $L_r$ | Reference Length |
| $M$ | Mach Number |
| $P$ | Static Pressure |
| $R$ | Radius of Curvature |
| $R_g$ | Gas Constant |
| $R_e$ | Reynolds Number |
| $S$ | Span |
| $T$ | Temperature |
| $U,V,W$ | Velocity Components |
| $X,Y,Z$ | Coordinates |
| | |
| $\gamma$ | Ratio Specific Heats |
| $\xi$ | Streamwise Vorticity |
| $\eta$ | Principle Normal Vorticity |
| $\rho$ | Density |
| $\phi_s$ | Secondary Velocity Potential |
| $\Psi_s$ | Secondary Stream Function |

Subscripts

| | |
|---|---|
| $r$ | Reference Condition |
| $I$ | Inviscid Flow |
| $S$ | Secondary Flow |
| $V$ | Viscous Flow |

# 8.0 FIGURES AND TABLES

TABLE I TEST CASE CONDITIONS

| Case No. = | 1 | 2 | 3 | 4 |
|---|---|---|---|---|
| Reynolds Number $R_e$ = | 1000 | 1000 | 940 | 940 |
| Mach Number M = | .1 | .25 | .1 | .1 |
| Temperature $^{o}R$ $T_r$ = | 416. | 416. | 416. | 416. |
| Pressure atm $P_r$ = | .25 | .25 | .25 | .25 |
| Density slug/$ft^3$ $\rho_r$ = | 7.66-04 | 7.66-04 | 7.66-04 | 7.66-04 |
| Viscosity $ft^2$/sec $V_r$ = | .0165 | .0143 | .0165 | .0165 |
| Velocity ft/sec $U_r$ = | 100. | 250. | 100. | 100. |
| Prandtl No. $P_R$ = | 1.0 | 1.0 | 1.0 | 1.0 |
| Span/Gap S/G = | 3.0 | 3.0 | 1.0 | 1.0 |
| R/D = | | | 14.0 | 14.0 |
| $RE_D$ = | | | 940. | 940. |
| Dean's Number K = | | | 251. | 251. |
| ARC Length (deg) $\theta$ = | | | 90. | 220. |

VANE PASSAGE GEOMETRY AND COMPUTED COORDINATE SYSTEM

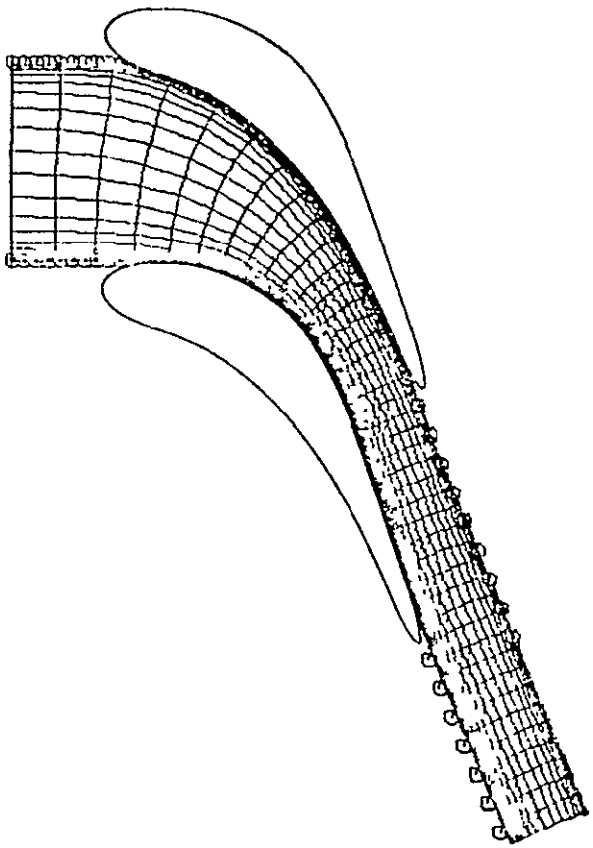

78-04-306-5

## CONTOURS OF STREAMWISE VORTICITY, $\xi$

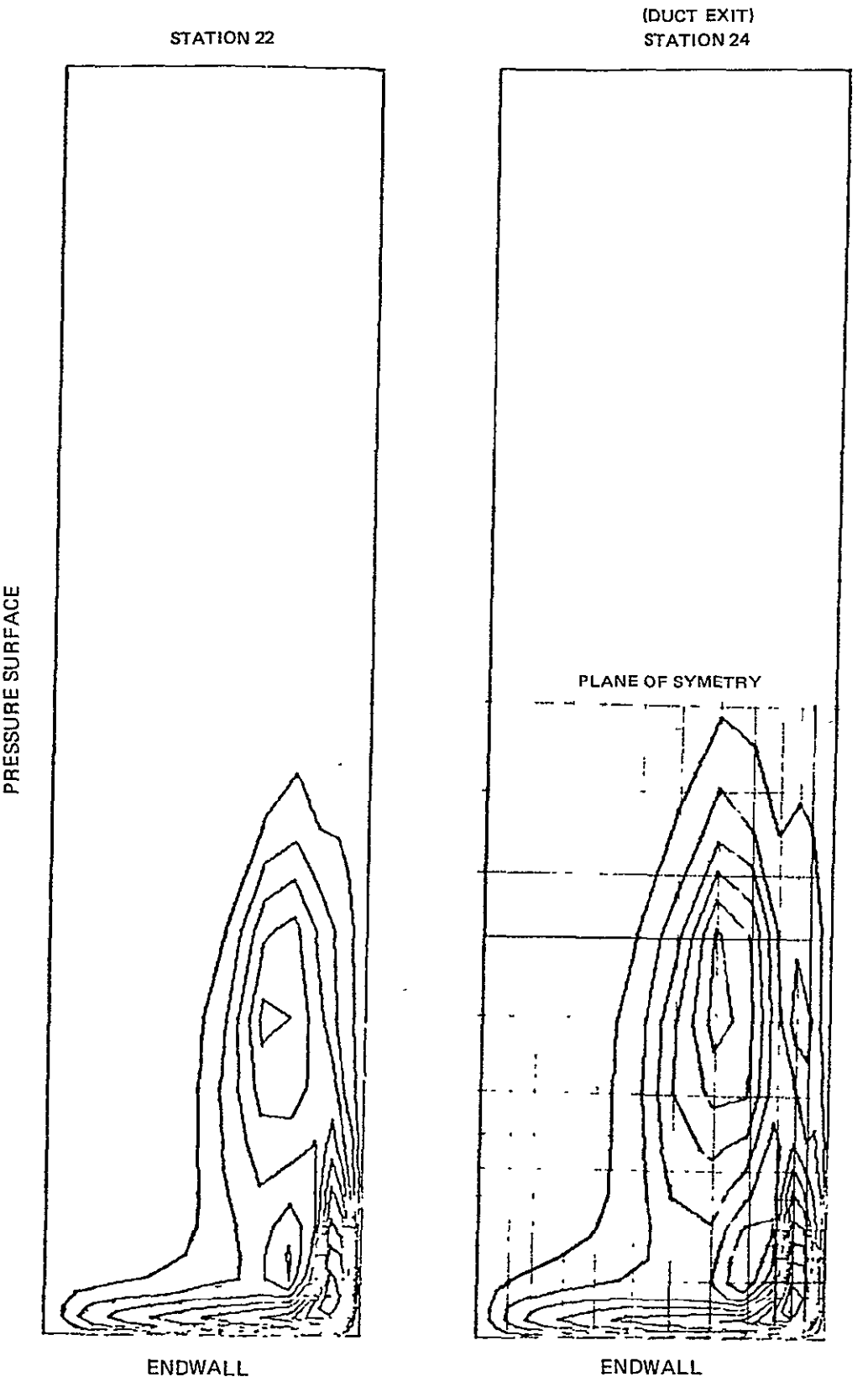


78-04-306-4

## STREAMWISE VORTICITY DISTRIBUTION AT (TURBINE) DUCT EXIT

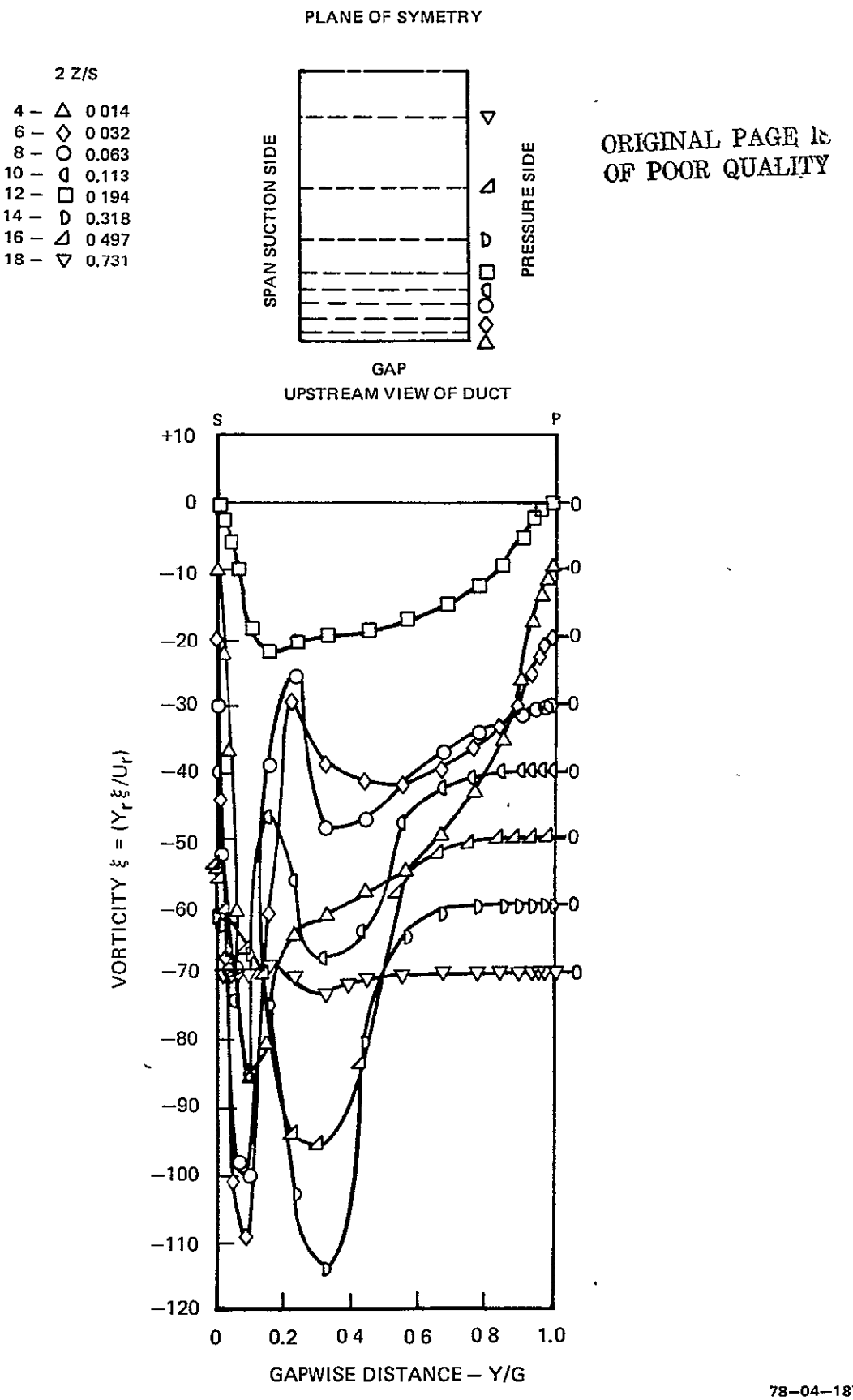


ORIGINAL PAGE IS
OF POOR QUALITY

# GAPWISE VELOCITY DISTRIBUTION FROM END WALL TO LINE OF SYMMETRY AT (TURBINE)DUCT EXIT

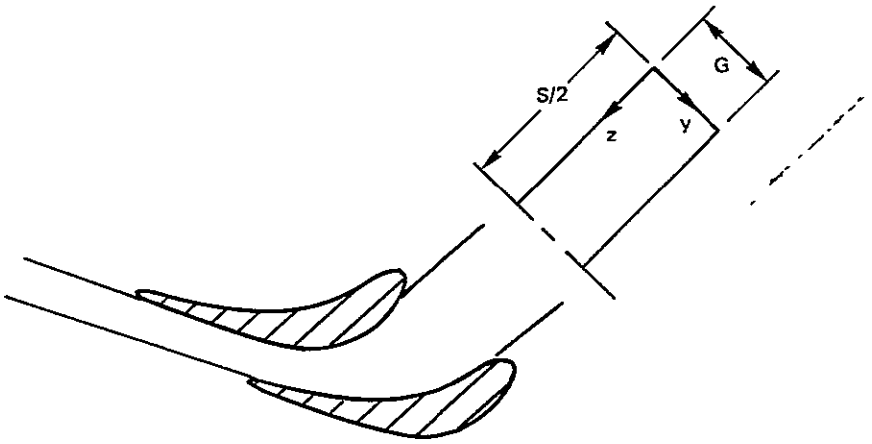


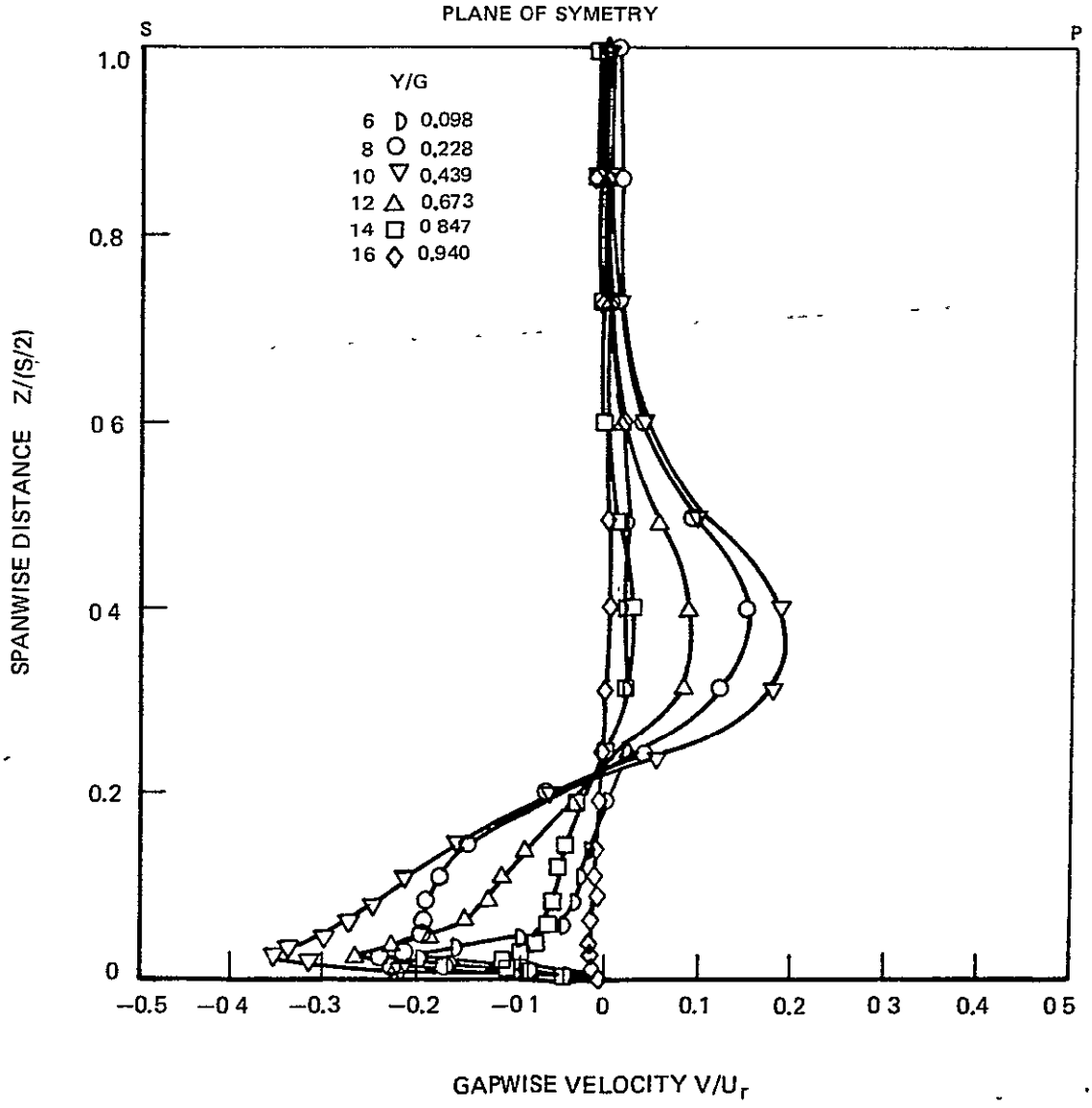


78–04–187–5

FIG. 5

## SPANWISE VELOCITY DISTRIBUTION FROM PRESSURE TO SUCTION SIDE AT (TURBINE) DUCT EXIT

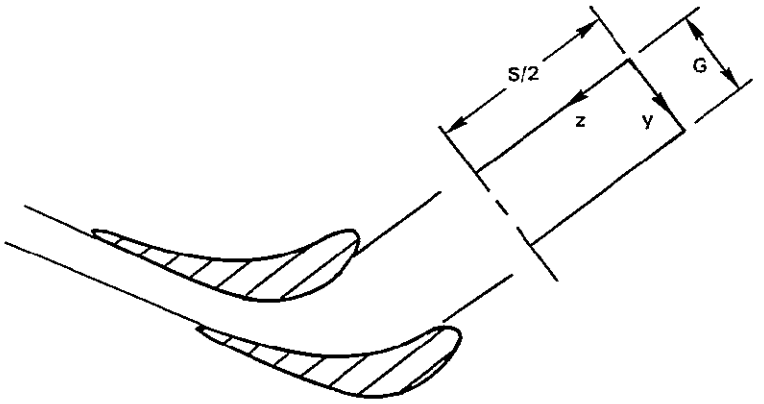


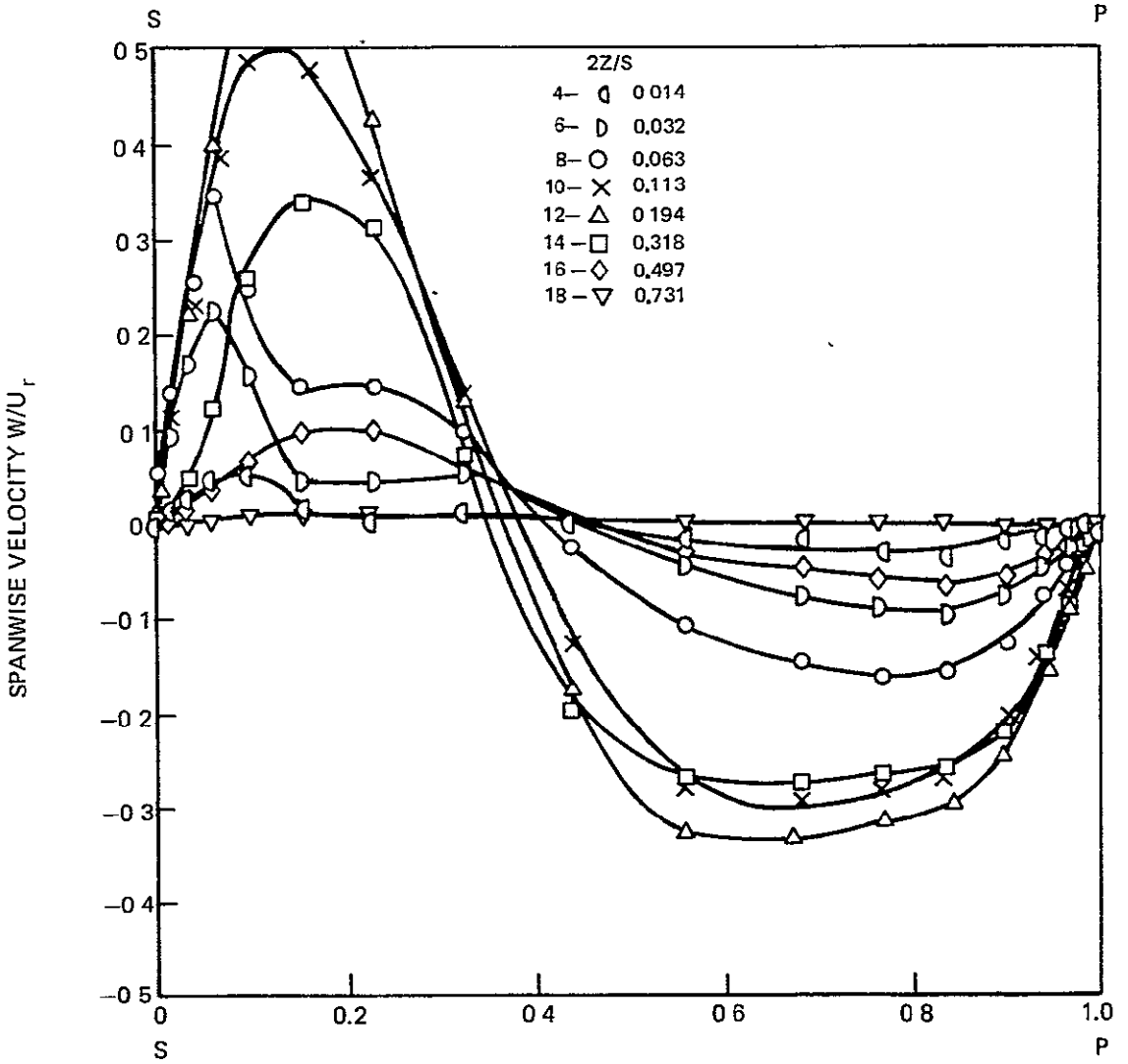


78–04–187–1

# STREAMWISE VELOCITY DISTRIBUTION AT (TURBINE) DUCT EXIT

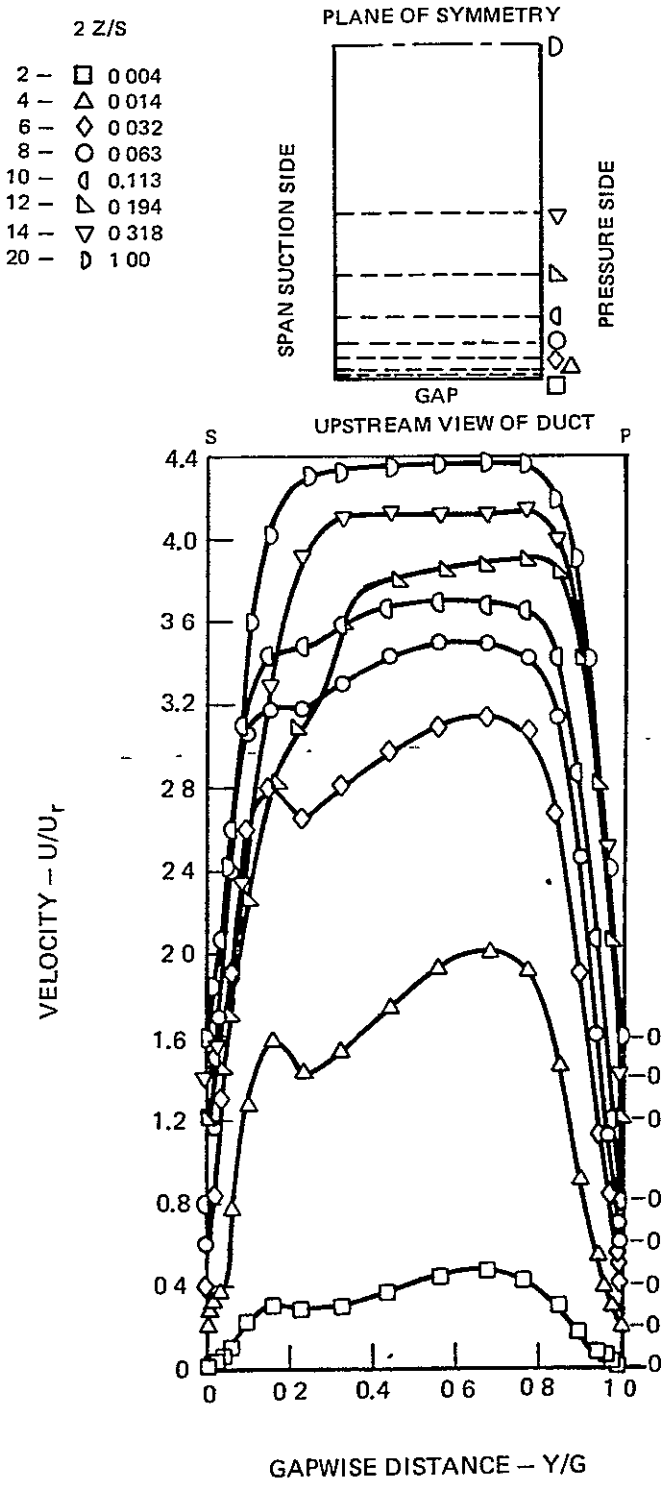


78–04–187–2

FIG 7

## LOSS DISTRIBUTION AT (TURBINE) DUCT EXIT

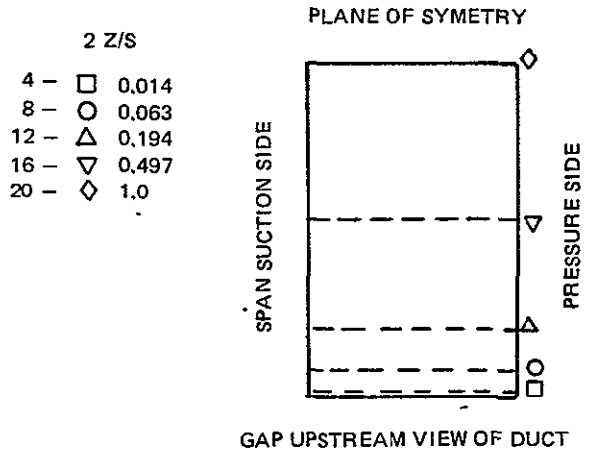


GAP UPSTREAM VIEW OF DUCT

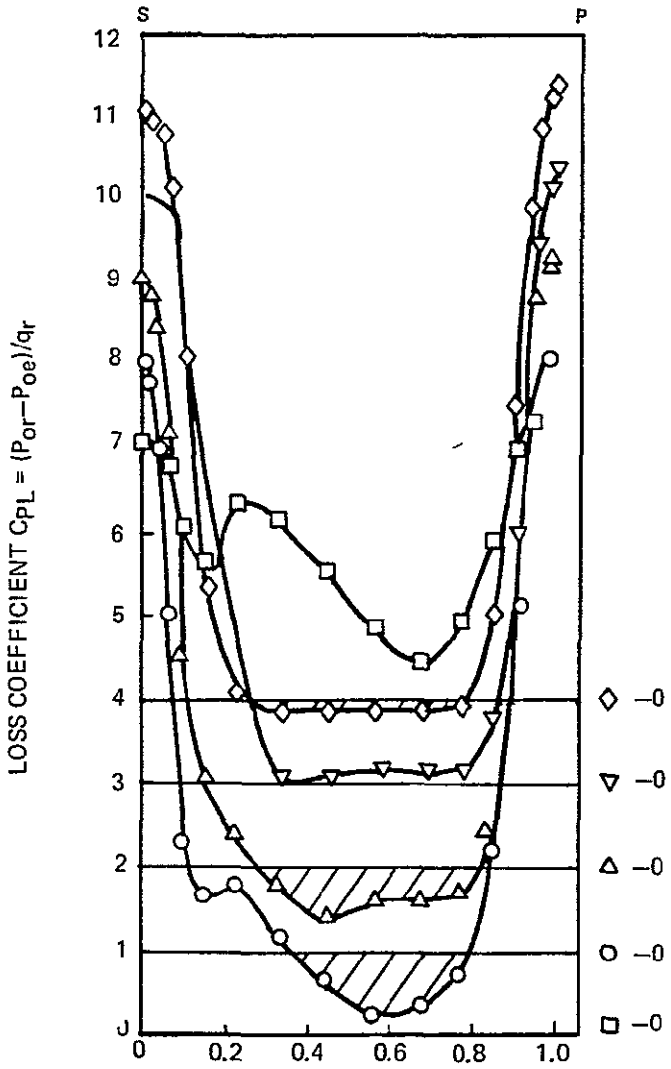


78–04–187–6

## GAPWISE WALL STATIC PRESSURE AT (TURBINE) DUCT EXIT

$$C_p - C_{p_o} = -\frac{2\nu}{U_r} \int_o^{Y_2} \frac{\partial \xi}{\partial Y_3} dY_2$$

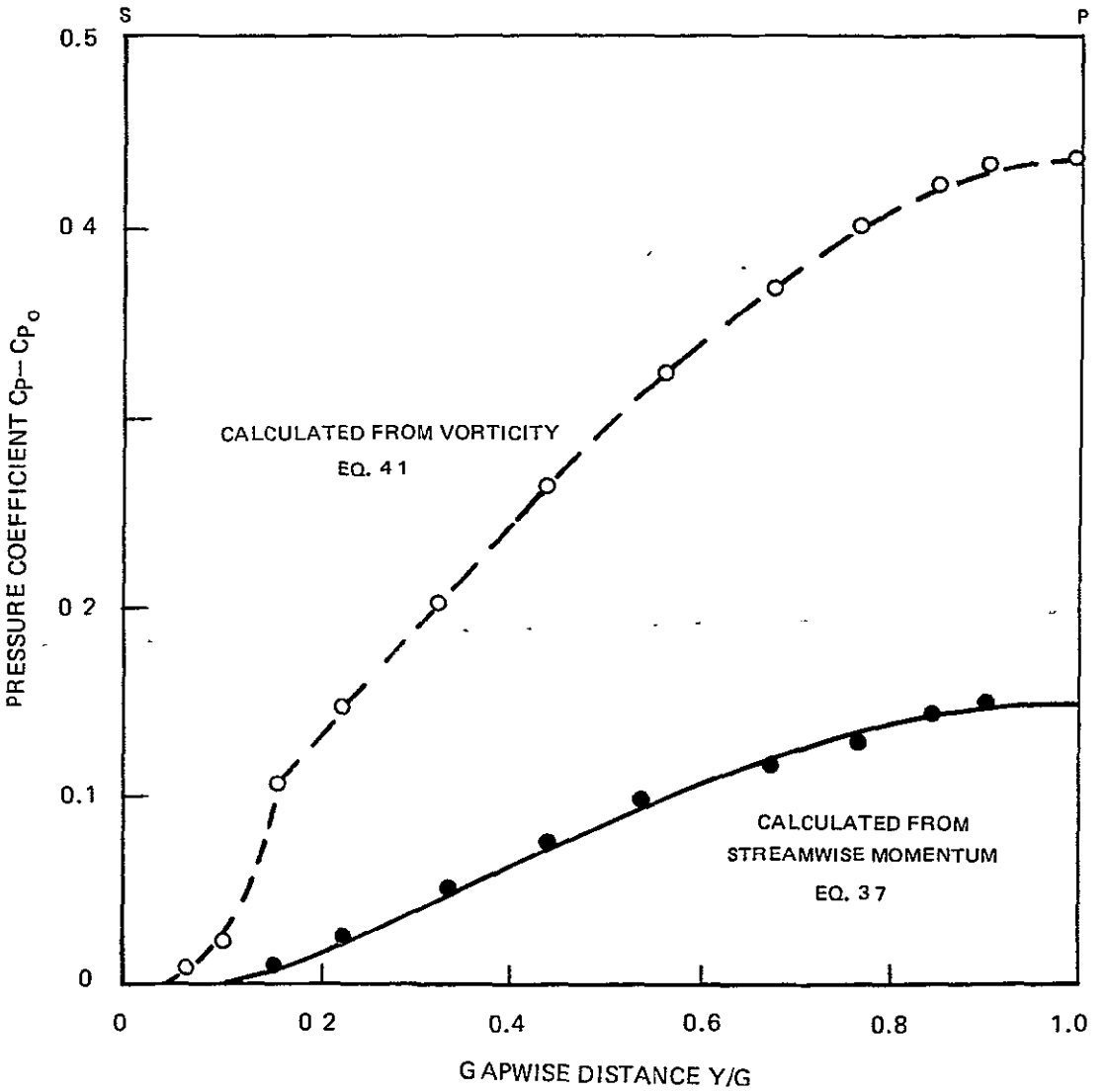


78-04-187-7

FIG. 9

DEPENDENCE OF LOSS DISTRIBUTION ON MACH NUMBER
FOR TURBINE END WALL DUCT

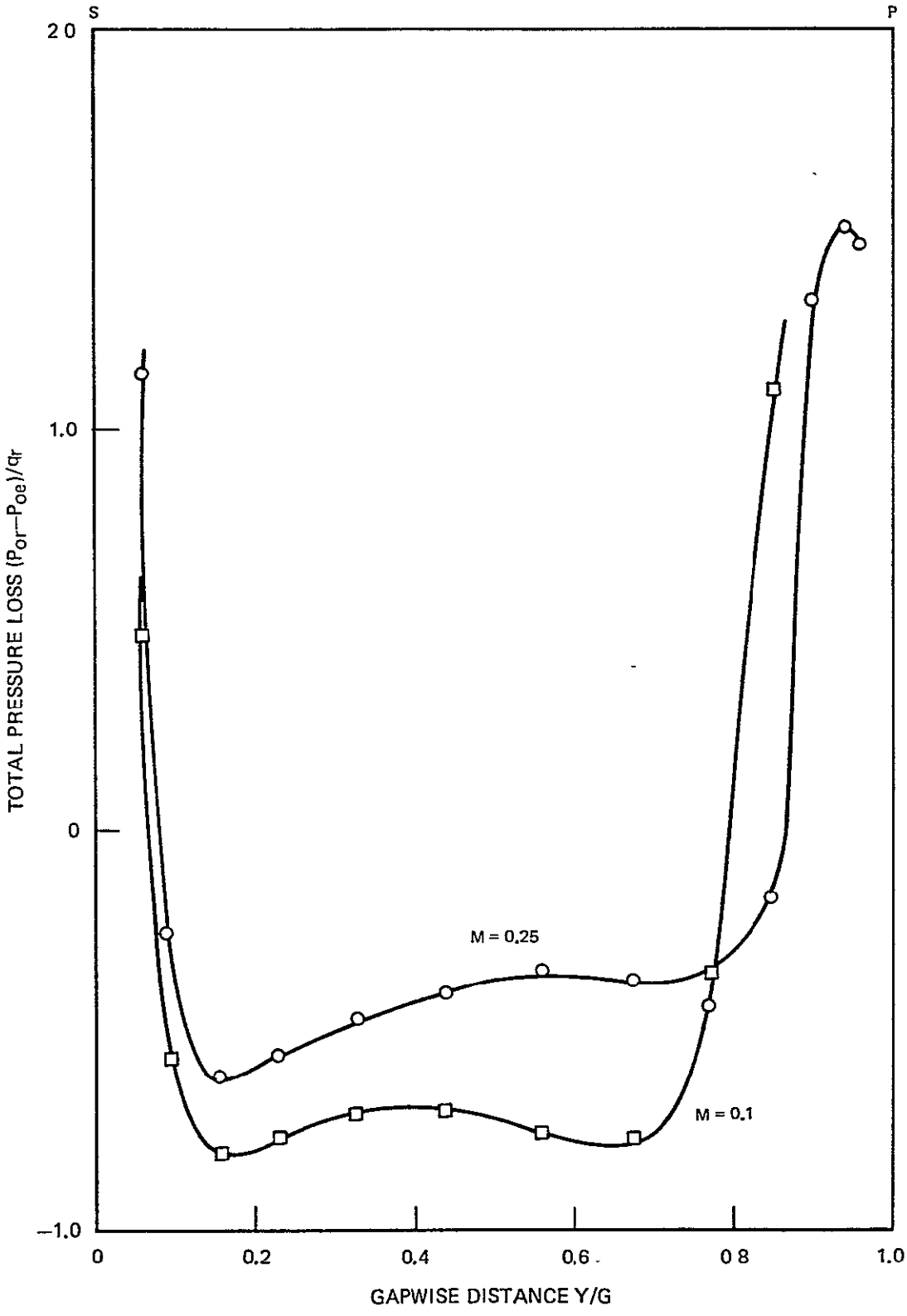


78–04–306–3

## GEOMETRY OF CURCULAR ARC DUCT

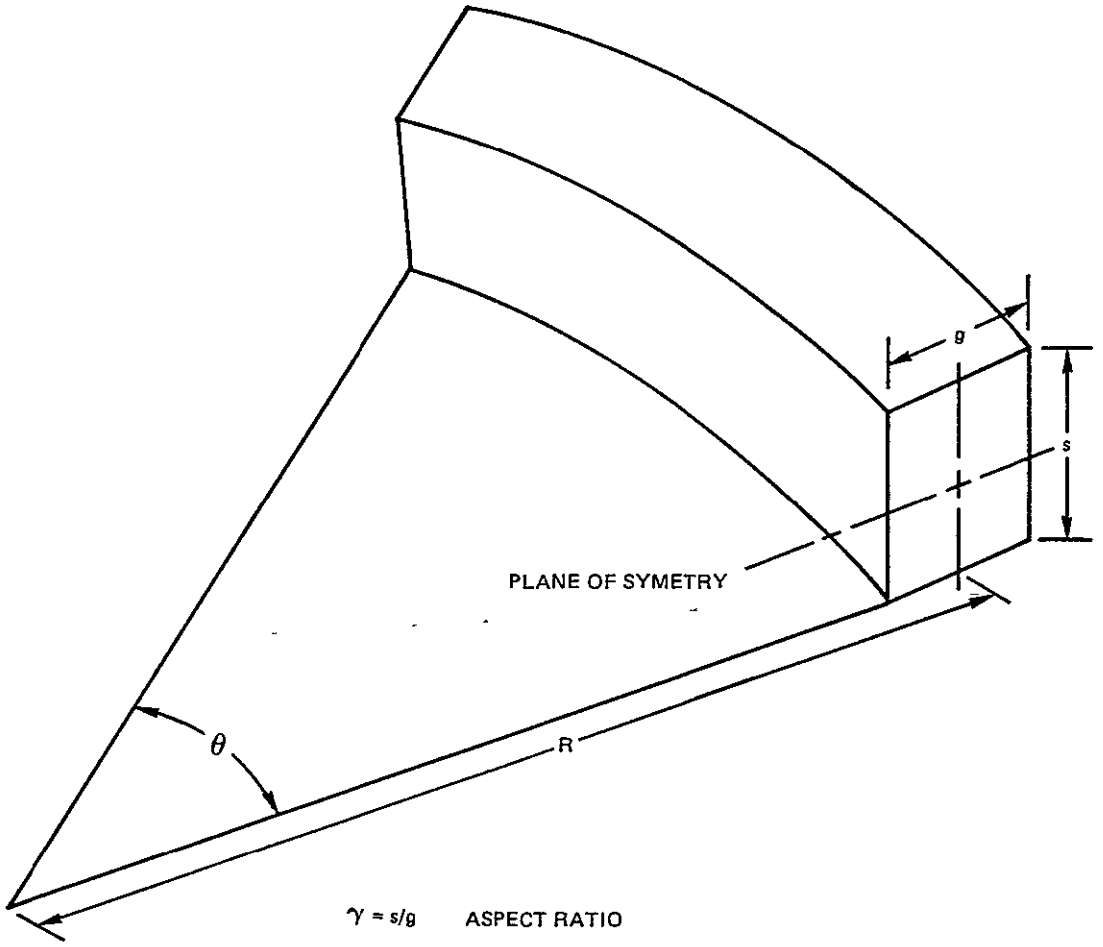


$\gamma = s/g$ ASPECT RATIO

$D = 2\,\frac{s \cdot g}{s + g}$ HYDRAULIC DIAMETER

$R_{eD} = UrD/\nu$ REYNOLDS NUMBER

$K = R_{eD}\sqrt{D/R}$ DEAN NUMBER



78-04-306-1

FIG. 11

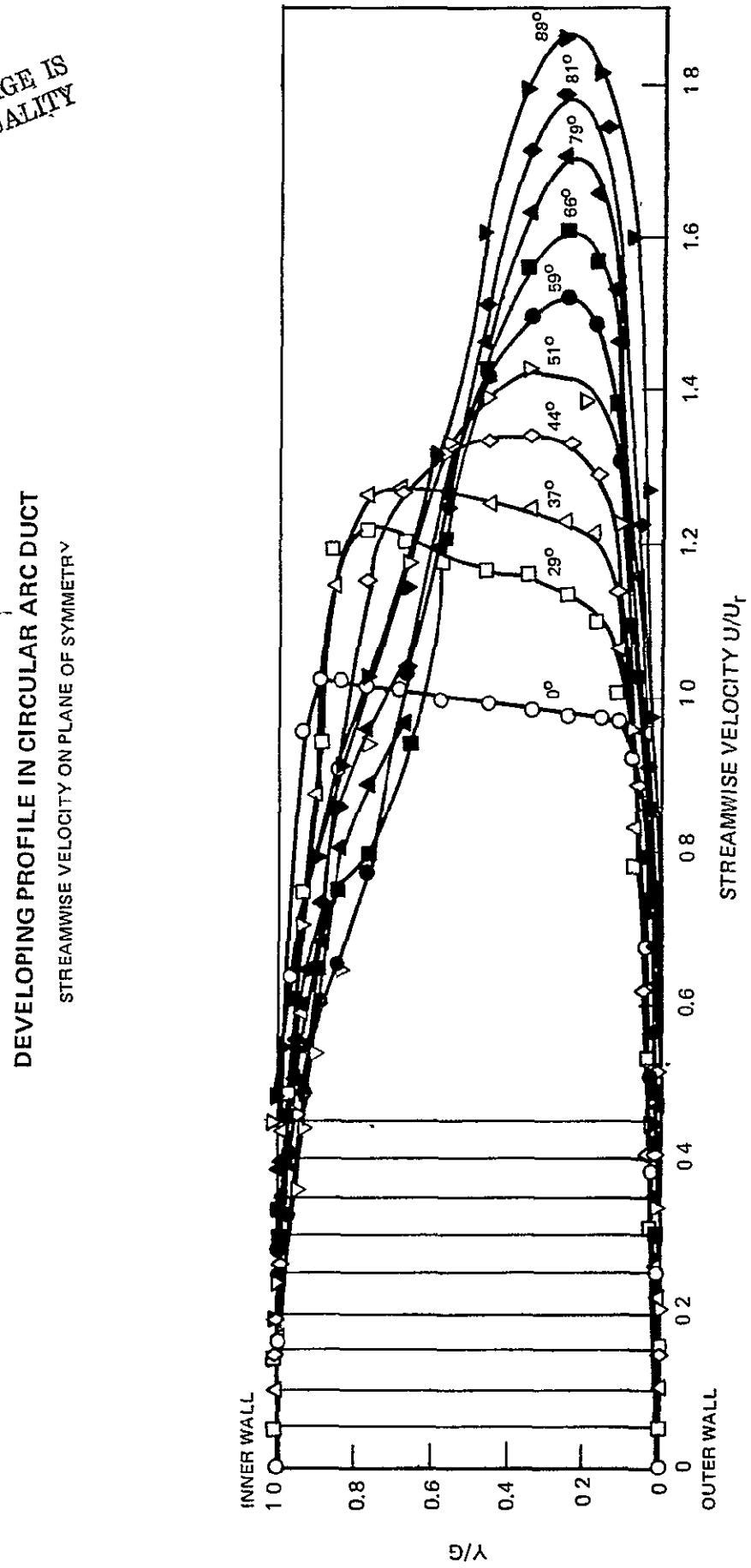


78-04-187-3

## STREAMWISE VELOCITY DISTRIBUTION ON PLANE OF SYMMETRY FOR CIRCULAR ARC DUCT

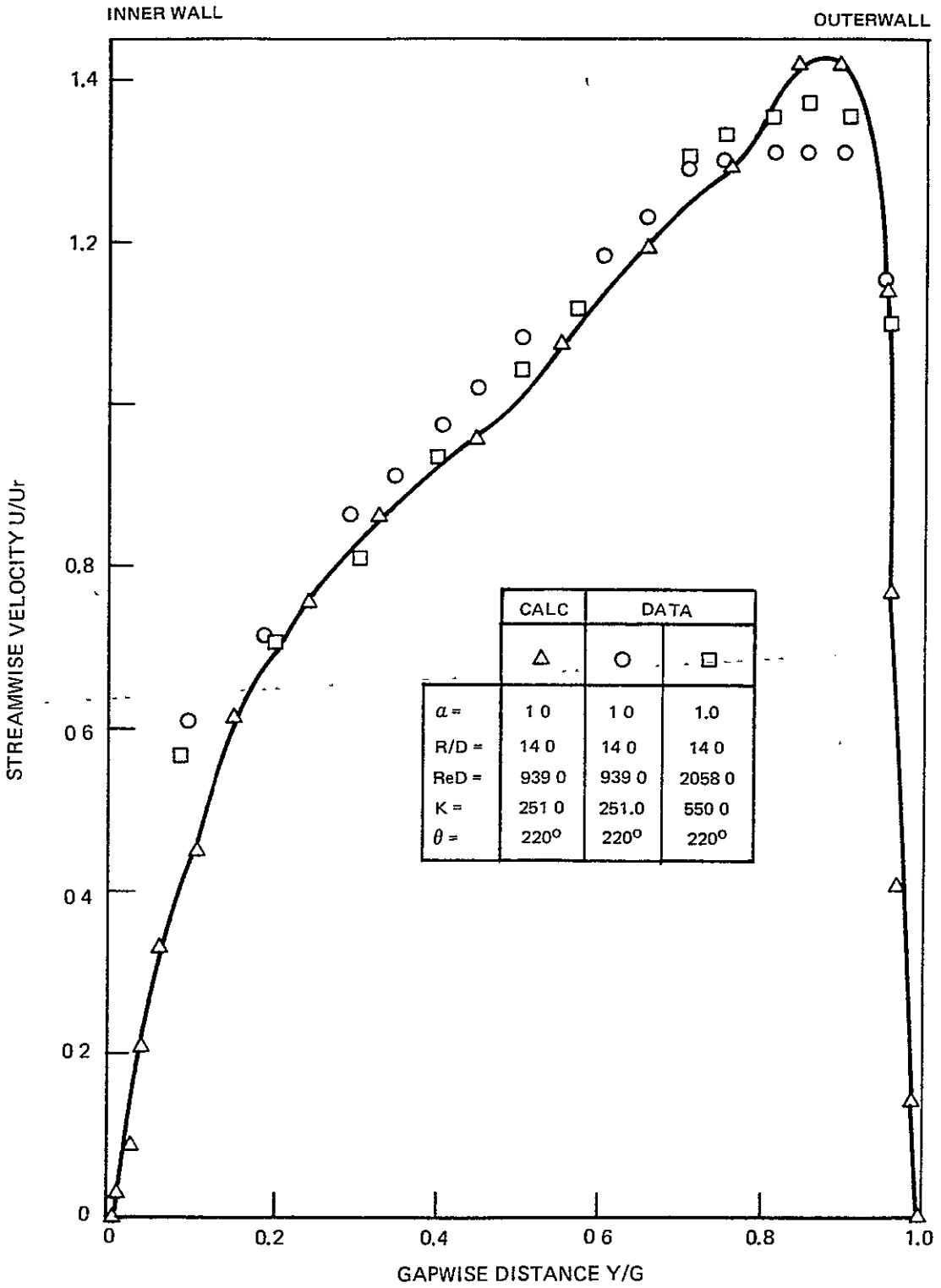


78-04-306-2

# 9.0 PROGRAM DESCRIPTION

The Turbine End-Wall Computer Program (TEWCP) consists of two separate computer codes: 1) coordinate calculation (GDCØØR), and 2) three-dimensional viscous calculation (PEPSIP). The GDCØØR code calculates an orthogonal coordinate system based on conformal mapping (Ref. 6). In addition, a separate code (GCCØØR) is provided to generate coordinates for circular arc ducts. The PEPSIP code is described in this report and the coordinate calculation in Ref. 6.

## 9.1 Run Stream

The PEPSIP computer code has no data card input. Each case must be treated separately and a new program constructed for each case. Most input parameters are set in subroutine INPUTS. Therefore the runstream for UNIVAC computers, requires compilation and construction of a new absolute code. Program GDCØØR and GCCØØR have data card input. The PEPSIP code also uses input data generated by GDCØØR describing the coordinates and stored on temporary or permanent files. Also depending on the PEPSIP options, there is a start/restart data file and an output plot data file. Therefore the runstream depends on the selected options.

Three runstreams are described below. Run 1 shows the normal runstream where the general coordinates and viscous calculation are completed in the same run. Run 2 shows the runstream for circular arc ducts. Run 3 shows the runstream in which the coordinates have been previously calculated and stored on a permanent file.

Run 1 General Coordinates

```
@ASG,A  QUAL*PLØTD., F111800                          ] Plot data file
@USE    8,QUAL*PLØTD.                                 ]

@ASG,T  9,0/50000/TRK/50000
@ASG,T  10.

@ASG,A  QUAL*RESTART.,D/100000/TRK/150000             ] Restart file
@USE    11,QUAL*RESTART.                              ]

@ASG,T  12,D/5000/TRK/5000
@ASG,T  13,D/5000/TRK/5000
@ASG,T  14,D/5000/TRK/5000

@ASG,A  QUAL*ADD.                                     ] Setup Coordinate
@COPY,A QUAL*ADD.GDCØR,TPF$.                          ] Calculation
@XQT    GDCØR                                         ]

    {input data                                       ]
    {note:  NDRUM = 10                                ]

@ASG,A  QUAL*PEPSIP.                                  ] Setup Viscous
@COPY   QUAL*PEPSIP,TPF                               ] Flow Calculation
@FOR,S  INPUTS,INPUTS,INPUTS                          ]

    {make temporary changes to                        ]
    {subroutine INPUTS                                ]

@MAP,SEN  MAPB,ABSA                                   ]
@XQT ABSA                                             ]

@FIN
```

Run 2 Circular Arc Duct

```
@ASG,A  QUAL*PLØTD., F///800                                  ] Plot data file
@USE    8,QUAL*PLØTD.                                         ]

@ASG,T  9,D/50000/TRK/50000
@ASG,T  10.

@ASG,A  QUAL*RESTART.,D/100000/TRK/150000                     ] Restart file
@USE    11,QUAL*RESTART.                                      ]

@ASG,T  12,D/5000/TRK/5000
@ASG,T  13,D/5000/TRK/5000
@ASG,T  14,D/5000/TRK/5000

@ASG,A  QUAL*ADD.                                             ] Setup Coordinate
@COPY,A QUAL*ADD.GDCØR,TPF$.                                  ] Calculation
@XQT    GDCØR                                                 ]

    {input data                                               ]
    {note:  NDRUM = 10}.                                      ]

@ASG,A  QUAL*PEPSIP.                                          ] Setup Viscous
@COPY   QUAL*PEPSIP,TPFS.                                     ] Flow Calculation
@FOR,S  INPUTS,INPUTS,INPUTS                                  ]

    {make temporary changes to }                              ]
    {subroutine INPUTS         }                              ]

@MAP,SEN  MAPB,ABSA                                           ]
@XQT ABSA                                                     ]

@FIN
```

Run 3 Stored Coordinates

```
@ASG,A    QUAL*PLØTD.,F///800
@USE      8,QUAL*PLØTD.

@ASG,T    9,D/50000/TRK/50000

@ASG,A    QUAL*CØØRF.
@USE      10,QUAL*CØØRF

@ASG,A    QUAL*RESTART.,D/100000/TRK/150000
@USE      11,QUAL*RESTART

@ASG,T    12,D/5000/TRK/5000
@ASG,T    13,D/5000/TRK/5000
@ASG,T    14,D/5000/TRK/5000

@ASG,A    QUAL*PEPSIP.
@CØPY     QUAL*PEPSIP., TPF$
@FØR,S    INPUTS,INPUTS,INPUTS

     make temporary changes to
     subroutine INPUTS

@MAP,SEN   MAPB,ABSA
@XQT  ABSA

@FIN
```

Plot data file

Coordinate data file

Setup Viscous Flow Calculation

## 9.2 Input for General Coordinates (GDCØØR)

Card No. 1 Title Card

| Name | Col. | Format | Comments: |
|---|---|---|---|
| Title | 1-72 | 12A6 | Any Alpha Numeric Characters |

Card No. 2 Option Card

| Name | Col. | Format | Comments: |
|---|---|---|---|
| JL(NS) | 1-2 | I2 | No. Streamwise Stations |
| KL | 3-4 | I2 | No. Streamlines |
| KDS | 5-6 | I2 | = 1 |
| JLPTS | 7-8 | I2 | No. Input Data Points |
| IDBG6 | 9-10 | I2 | = 0 No Print, = 1 print coordinates |
| NDRUM | 11-12 | I2 | Disc Storage Unit No. = 10 |
| LFILE | 13-14 | I2 | = 0 Tape Storage |
| DDS | 15-24 | F10.0 | Mesh Distortion Parameter |
| DUCTI (1) | 25-34 | F10.0 | Duct Length (ft) |
| DUCTI (2) | 35-44 | F10.0 | No. Knots |

Card No. 3 through 2 JLPTS/8 + 5

| Name | Col. | Format | Comments: |
|---|---|---|---|
| RD1I (J) | 1-80 | 8F10.0 | OD Duct Radius (ft)(J=1,JLPTS) |
| RD2I (J) | 1-80 | 8F10.0 | ID Duct Radius (ft)(J=1,JLPTS) |

## 9.3 Output for General Coordinates

| | | |
|---|---|---|
| USCALE | $U_s$ | Metric Normalizing Factor |
| EPS (1) | $\epsilon_1$ | Roberts Transformation Parameter |

## 9.4 Input for Circular Arc Duct

Card No. 1 Title Card

| Name | Col. | Format | Comments: |
|---|---|---|---|
| Title | 1-72 | 12A6 | Any Alpha Numeric Character |

Card No. 2 Option Card

| Name | Col. | Format | Comments: |
|---|---|---|---|
| JL | 1-10 | I10 | No. Streamwise Stations |
| KL | 11-20 | I10 | No. Streamlines |
| KDS | 21-30 | I10 | = 1 |
| JDBG6 | 31-40 | I10 | = 0 No Print, = 1 Print Coordinate |
| NDRUM | 41-50 | I10 | = 10 |
| DDS | 51-60 | F10.0 | Mesh Distortion Parameters |

Card No. 3 Parameter Card

| Name | Col. | Format | Comments: |
|---|---|---|---|
| DUCTI (1) | 1-10 | F10.0 | $d_1$ |
| DUCTI (2) | 11-20 | F10.0 | $d_2$ |
| DUCTI (3) | 21-30 | F10.0 | $d_3$ |
| DUCTI (4) | 31-40 | F10.0 | $d_4$ |
| DUCTI (5) | 41-50 | F10.0 | $d_5$ |
| DUCTI (6) | 51-60 | F10.0 | $d_6$ |
| DUCTI (7) | 61-70 | F10.0 | $d_7$ |
| DUCTI (8) | 71-80 | F10.0 | $d_8$ |

## 9.5 Output for Circular Arc Duct

| | | |
|---|---|---|
| USCALE | $U_s$ | Metric Normalizing Factor |
| EPS (1) | $\epsilon_1$ | Roberts Transformation Parameter |

## 9.5 Input for PEPSIP

| Name | Symbol | Comment |
|---|---|---|
| CP | $C_p$ | Specific Heat (ftlb/slug/$^oR$) |
| EPS (1) | $\epsilon_1$ | Roberts Parameter Gapwise |
| EPS (2) | $\epsilon_2$ | Roberts Parameter Spanwise |
| EZERO | $E_o$ | Reference Energy $1/((r-1)M_r^2) + 1/2$ |
| GAMMA | $\gamma$ | Ratio Specific Heats |
| IRSTIN | = 0 | No Restart |
| | > 0 | Starting Station |
| NFILE | = 1 | No Restart |
| | > 0 | Sequence Number from Last Printout |
| NS | | Last Station |
| NSAVE | = 0 | No Restart |
| | > 0 | Sequence Number from Last Printout |
| PRL | $P_{RL}$ | Note Set Equal to One in Code |
| PRT | $P_{RT}$ | |
| RG | R | Gas Constant (ftlb/slug/$^oR$) |
| RZERO | $\rho_r$ | Reference Density |
| SØUND | C | Reference Speed of Sound (ft/sec) |
| TSTAG | $T_s$ | Reference Stagnation Temperature ($^oR$) |
| TWALL | $T_w$ | Wall Temperature ($^oR$) |
| TZERO | $T_r$ | Reference Temperature ($^oR$) |
| USCALE | $U_s$ | Metric Normalizing Factor |
| UZERO | $U_r$ | Reference Velocity |
| VISCØS | $\mu_r$ | Reference Kinematic Viscosity |
| YS (2,1) -YS (1,1) | g | Inlet Gap (ft) |
| YS (2,2) -YS (1,2) | S/2 | Inlet Span (ft) |
| X(2)-X(1) | $\Delta X$ | Initial Step Size |
| YZERO | $Y_r$ | Reference Length (Set = 1.0) |

## 9.6 Output For PEPSIP

| Name | Symbol | Comment |
|---|---|---|
| X | X | Streamwise Station |
| Y | Y | Gapwise Station |
| Z | Z | Spanwise Station |
| U-VEL | $U/U_r$ | Streamwise Velocity |
| VCØMP | $V/U_r$ | Gapwise Velocity |
| WCØMP | $W/U_r$ | Spanwise Velocity |
| RHØ | $\rho/\rho_r$ | Density |
| VØR | $\xi Y_r/U_r$ | Streamwise Vorticity |
| STREAM | $\Psi/(V_r U_r)$ | Secondary Stream Function |
| CP/2 | $(P-P_r)/(1/2\rho_r U_r^2)$ | Pressure Coefficient |
| TSTAT | $T/T_r$ | Static Temperature |

## 9.7 PEPSIP/GDCØØR Interface

Let (X,Y,Z) be the generalized orthogonal coordinates used in the PEPSIP code and (s,n) be the two dimensional generalized orthogonal coordinates computed by GDCØØR as described in Ref. 6. The coordinates are matched as follows:

$$Y_r h_x d_x = r_r dS/V \tag{9.7.1}$$

$$Y_r h_x d_y = r_r dn/V \tag{9.7.2}$$

where $r_r$ is the normalizing length scale used on GOCØØR and V is the inverse of the metric scale coefficient, $Y_r$ is the length scale in PEPSIP. Then (x;s) is the streamwise coordinate matching pair and (y;n) is the gapwise coordinate matching pair. The spanwise coordinate is generated by extension

$$Y_r h_z d_z = dt/V(s,n) \tag{9.7.3}$$

The matching of length scales and metric coefficients is done on the coordinates defined at the inlet. Thus with $V_r$ a metric normalizing factor, duct arc lengths at the inlet are given by,

$$X(2)-X(1) = Y_r h_x \Delta X = r_r \Delta S/V_r \tag{9.7.4}$$

$$YS(2,1)-YS(1,1) = Y_r \int_{y_1}^{Y_z} h_y d_y = r_r \int_{n_1}^{n_z} \frac{dn}{V_r} = r_r/V_r \tag{9.7.5}$$

$$YS(2,2)-YS(1,2) = Y_r \int_{Z_1}^{Z_2} h_z d_z = r_r \int_{t_1}^{t_2} \frac{dt}{V_r} \tag{9.7.6}$$

Then we have using (9.7.2) and (9.7.5) with $V_r$ constant,

$$h_x = h_z - h_y = \frac{r_r}{V} \frac{1}{Y_r} = \frac{YS(2,1)-YS(1,1)}{Y_r} \cdot \left( \frac{V_r}{V} \right) \tag{9.7.7}$$

Finally since V is the potential flow velocity, the incompressible pressure coefficient is

$$C_p = 1 - \left( \frac{V}{V_r} \right)^2 \tag{9.7.8}$$

Then with the PEPSIP length scale $Y_r = 1$, the coordinates are uniquely defined by

X(2)-X(1) = first step size in marching direction (ft)

YS(2,1)-YS(1,1) = inlet gap (ft)

YS(2,2) - YS(1,2) = inlet height (ft)

$U_s = V_r$ = Metric normalizing factor.

# 10.0 APPENDIX

## An Approximate Analysis for Three-Dimensional Viscous Subsonic Flows with Large Secondary Velocities

by

W. R. Briley and H. McDonald

The following section contains results from an analytical investigation of turbine endwall flow and heat transfer, performed by Scientific Research Associates, Inc., under subcontract to United Technologies Research Center.

# FOREWORD

The following report contains results from an analytical investigation of turbine endwall flow and heat transfer, performed by Scientific Research Associates, Inc., under subcontract to United Technologies Research Center. The investigation was initiated while the authors were affiliated with United Technologies Research Center and completed under Subcontract.

# An Approximate Analysis for Three-Dimensional Viscous Subsonic Flows with Large Secondary Velocities

## INTRODUCTION

An approximate analysis is developed for a class of three-dimensional subsonic viscous flows at high Reynolds number, which have a predominant primary flow direction with secondary flow in transverse planes. A key restriction of the analysis is that once a primary flow direction is established, reversed flow in the primary flow direction (flow separation) does not occur. As a consequence, the analysis is not intended for application in geometries having sharp curvature in the primary flow direction. However, the analysis is specifically designed for flow configurations having large turning as a result of strong geometric curvature, $R = O(1)$ but not sharp $R = O(\varepsilon)$ curvature in the primary flow direction, R being the geometric radius of curvature. Such flows are common in turbomachinery applications, where internal flow passages are usually aerodynamically smooth. The problem of primary interest here is the flow in turbine blade passages, and particularly the strong secondary flows and corner vortices associated with the endwall regions.

The present analysis synthesizes concepts from potential flow theory, secondary flow theory, and from an extension of three-dimensional boundary layer theory in a manner which allows efficient solution by forward-marching numerical integration techniques, given only knowledge of the potential flow. Repeated and costly (iterative) sweeping of the entire three-dimensional flow field is not necessary to obtain a valid approximation to the flow. As a consequence, numerical solution of the derived governing equations will generally require considerably less computer time than would a solution of the full three-dimensional Navier-Stokes equations. An *a priori* potential flow solution nevertheless accounts at least approximately for the important elliptic influence of downstream boundary conditions and determines the primary flow direction. One might consider a possible variation of the analysis which would employ an *a priori* inviscid flow not from a potential flow solution but from a solution of the rotational inviscid flow equation. This would result in a considerable increase in computational effort since for the same number of mesh points solving the rotational inviscid flow equations takes only slightly less effort than solving the full Navier-Stokes equations. On the other hand, much less effort is required to solve the potential equation. Finally, the

analysis recognizes that a pressure field determined solely from potential flow theory is probably an inadequate representation of the pressure field when large confined secondary flows are present.

## BACKGROUND

Because of their complexity, and particularly the interaction which occurs between primary and secondary flows and between viscous and inviscid regions, three-dimensional viscous flows, particularly confined flows in highly curved ducts, have been extremely difficult to analyze, short of numerical solution of the complete Navier-Stokes equations. This latter alternative is of course definitive but, in three dimensions, it requires a great deal of computational effort. The present analysis, although approximate, is much more economical in terms of computer time. Approximate methods, which treat the flow partly by forward marching and partly as fully elliptic, have been proposed recently by Dodge [1] and by Pratap & Spalding [2]. These methods require iterative sweeping of the entire three-dimensional flow field, however, and consequently the computer time required tends to be comparable with that needed for solution of the complete Navier-Stokes equations, without approximation. The present analysis is an outgrowth of and to some extent a synthesis of previous work involving widely differing approaches. Highlights from this previous work are briefly reviewed here.

### Rotational Inviscid Flow Theory

Rotational inviscid flow theory has provided considerable insight into the behavior of some secondary flows, and in many cases can provide quantitative predictions. For flows with large turning, Squire & Winter [3] first proposed a widely used inviscid "secondary flow approximation" which governs the generation of streamwise vorticity due to turning. Secondary flow theory and its applications have been reviewed by Hawthorne [4], Horlock & Lakshminarayana [5] and Lakshminarayana & Horlock [6]. Stuart & Hetherington [7] have computed solutions to the full incompressible, rotational inviscid equations of motion for flow through a curved duct. Treatment of viscous effects, however, has been difficult, although the relevant governing equations are known. Hawthorne [4] points out the necessity of defining a "cut-off velocity" near walls, to exclude the viscous region, and that this can have a major effect on the predictions of secondary flow theory. Techniques for computing three-dimensional boundary layers are available (cf, Nash & Patel [8]); however, three-dimensional boundary layer theory is not valid in viscous corner regions, and the patching or interfacing of boundary layer and rotational inviscid regions is not at all straightforward.

Extended Boundary Layer Analysis

Patankar & Spalding [9], Caretto, Curr & Spalding [10], and Briley [11] have suggested numerical methods for solving approximate governing equations which represent an extension of concepts from three-dimensional boundary layer theory. In these studies, solutions were computed for laminar incompressible flow in straight ducts with rectangular cross sections. The governing equations were solved by forward-marching integration in a primary flow coordinate direction while retaining viscous stresses in both transverse coordinate directions as opposed to only one direction for three-dimensional boundary layer theory. Viscous diffusion in the primary or streamwise direction is neglected as in conventional three-dimensional boundary layer theory. Unlike conventional boundary layer theory, however, the approximate governing equations are solved in the inviscid region as well as the viscous region. In addition to neglecting streamwise diffusion, the pressure is divided into an inviscid pressure "imposed", for example, by an irrotational flow, and a pressure correction due to viscous effects. The "viscous" pressure is treated differently in the streamwise and transverse momentum equations (an inconsistency) to permit solution by forward marching integration. Despite the inconsistent treatment of pressure gradients, these so-called "parabolic flow" methods gave reasonable predictions for flow in straight rectangular ducts. Ghia, Ghia & Studerus [12] also obtained reasonable predictions for flow in a "polar" duct whose cross sections are annular sectors. Recently, as part of a comprehensive study of entry flow in straight rectangular ducts, Rubin & Khosla [13] presented their own analysis and numerical method for the "fully viscous region". Their method is an extended boundary layer method in the present terminology.

Although the general approach of [9-13] produces reasonable results for flow in straight ducts, only very small secondary flows are present in such cases. Nevertheless, this approach has been used to compute moderate secondary flows generated by a moving wall [9], by a transverse buoyancy force [11], and in mildly curved pipes [14] and curved rectangular ducts [15]. In the fully-developed flow region, these results generally agree with other fully-developed solutions computed without approximation. Very little is known about the accuracy of these solutions in the developing flow region. It is not expected that these analyses as they presently exist would produce reasonable results for developing flows in ducts with large turning producing strong secondary flows, the problem of present concern. As a consequence, the present investigation was undertaken and had as its main goal the synthesis of results from "extended" boundary layer theory and classical secondary flow theory.

## ANALYSIS

### Outline

The present analysis is based on the decomposition of the overall velocity vector field $\bar{U}$ into "inviscid" components $\bar{U}_I$ and $\bar{U}_s$ which satisfy slip conditions, and a "viscous" component $\bar{U}_v$ which corrects for no-slip conditions at wall boundaries. The overall velocity is determined from the superposition

$$\bar{U} = \bar{U}_I + \bar{U}_s + \bar{U}_v \tag{10.2.1}$$

Elements of the velocity decomposition are briefly described below:

(1) $\bar{U}_I$ is the irrotational velocity field determined from a potential flow solution in the geometry under consideration. Depending on the particular application, approximate downstream conditions such as the commonly used "Kutta condition" may be required. The direction of $\bar{U}_I$ is then taken as the "primary flow direction". Curvilinear surfaces of constant potential may be taken as the transverse "secondary flow" planes, although this is not essential.

(2) $\bar{U}_s$ is a secondary flow velocity field which is further decomposed into a solenoidal component $\bar{U}_\psi$ and an irrotational component $\bar{U}_\phi$. $\bar{U}_\psi$ by definition has zero divergence and is determined from an approximate application of secondary flow theory, under assumptions less restrictive than those of the now classical "secondary flow approximation" of Squire & Winter [3]. Briefly, $\bar{U}_\psi$ is obtained from the solution of an approximate equation governing the growth and development of streamwise vorticity, followed by approximate vector potential calculations in curvilinear transverse secondary flow planes. The troublesome "velocity cut-off problem" of applications of inviscid secondary flow theory, mentioned by Hawthorne [4], is avoided by the retention of viscous terms. The irrotational component $\bar{U}_\phi$ ensures that the overall velocity field satisfies continuity and is obtained from approximate scalar potential calculations in curvilinear transverse secondary flow planes.

(3) $\bar{U}_v$ is a viscous velocity correction for no-slip conditions, computed under the influence of "imposed" pressure gradients determined by the superposition of $\bar{U}_I$ and $\bar{U}_s$.

Computationally, $\bar{U}_I$ is determined by an *a priori* elliptic potential flow calculation, whereas $\bar{U}_s$ and $\bar{U}_v$ are computed simultaneously by a coupled forward-marching numerical integration procedure. It is unnecessary to sweep the three-

dimensional flow field iteratively to obtain a valid approximate solution, although such a procedure is possible and may possibly improve the flow predictions. A key feature of the present analysis is that the pressure gradients associated with large secondary flows are determined a posteriori using approximations to these secondary velocities. This is necessary since although velocity is sufficient to determine pressure gradients from the momentum equations, a knowledge of pressure is insufficient to determine velocity, since velocity must satisfy continuity in addition to the momentum equations. Finally, although the present analysis can be easily extended to give a more comprehensive treatment of compressibility effects, at present compressibility is accounted for only through the use of the perfect gas equation of state in the imposition of the streamwise pressure gradients.

Primary Flow and Transverse Secondary Flow Planes

The primary flow is taken as the potential flow past the geometry in question. Thus,

$$\bar{U}_I = \nabla \phi_I \tag{10.2.2}$$

and from continuity,

$$\nabla \cdot \bar{U}_I = \nabla^2 \phi_I = 0 \tag{10.2.3}$$

The potential flow $\bar{U}_I$ can be determined either analytically or by numerical computation in some convenient coordinate system. The direction of $\bar{U}_I$ is taken as the primary flow direction. The unit vector $\bar{i}_p$ in the primary flow direction is given by

$$\bar{i}_p = \bar{U}_I / U_I \tag{10.2.4}$$

where velocity magnitude is denoted U and defined by

$$U \equiv \left| \bar{U} \right| \equiv (\bar{U} \cdot \bar{U})^{1/2} \tag{10.2.5}$$

It is also necessary to specify transverse secondary flow planes, which may be curvilinear. The unit vector normal to the secondary flow planes is denoted $\bar{i}_n$. Curvilinear planes of constant potential $\phi_I$ are an obvious but not essential

choice for the secondary flow planes, and in this case, $\bar{i}_n = \bar{i}_p$.

Secondary Flow Velocity Components

The solenoidal component $\bar{U}_\psi$ of the secondary velocity $\bar{U}_s$ is determined from an approximate application of secondary flow theory. From Horlock & Lakshminarayana [5] the equation governing the growth of streamwise vorticity for incompressible flow is

$$\frac{\partial}{\partial s}\left(\frac{\xi}{V}\right) = -\frac{2\eta}{VR} + \frac{\nu}{V^2}\left[\bar{s}\cdot\nabla^2\bar{\Omega}\right] \qquad (10.2.6)$$

where s is distance along a streamline, $\bar{s}$ is the unit vector tangent to a streamline, $\bar{\Omega}$ is the vorticity vector, $\xi$ is vorticity in the direction of $\bar{s}$, V is velocity magnitude, R is the local radius of curvature of a streamline, $\eta$ is transverse vorticity in the direction of R, and $\nu$ is kinematic viscosity. Equation (10.2.6) is exact and involves no approximation.

To obtain $\xi$ and subsequently $\bar{U}_\psi$, (10.2.6) is solved subject to the following approximations:

(1) $\xi$ is taken to be vorticity in the direction of the primary potential flow streamlines, i.e., $\xi_s = \xi(\bar{i}_p \cdot \bar{s}) \doteq \xi$

(2) s is taken to be distance in the direction of $\bar{U}_I + \bar{U}_s$, i.e.,

$$\frac{\partial}{\partial s} \doteq \frac{(\bar{U}_I+\bar{U}_s)}{|\bar{U}_I+\bar{U}_s|}\cdot\nabla \qquad (10.2.7)$$

Note that the inclusion of $\bar{U}_s$ in the secondary flow convective operator is a key feature of the present analysis, since this is the mechanism whereby streamwise vorticity in a curved blade passage is transported into the suction surface - endwall corner where it becomes the well-known corner vortex.

(3) V is taken to be the computed streamwise velocity magnitude, i.e., $V \doteq \bar{i}_p \cdot (\bar{U}_I + \bar{U}_s + \bar{U}_v)$.

(4) R is taken to be the local principal radius of curvature of a primary flow streamline.

(5) $\eta$ is taken to be the transverse vorticity in the direction of R as computed from V.

(6) The bracketed viscous diffusion term in (10.2.6) is replaced by an expression representing diffusion only in the transverse secondary flow planes: diffusion in the streamwise direction normal to these planes is neglected. This is

accomplished by replacing the bracketed term in (10.2.6) by

$$-\bar{i}_n \cdot (\nabla \times \nabla \times \xi_n \bar{i}_n) \doteq \bar{s} \cdot \nabla^2 \bar{\Omega} \tag{10.2.8}$$

where $\xi_n$ is the projection of $\xi_s \bar{i}_p$ onto $\bar{i}_n$, i.e., $\xi_n = \xi_s (\bar{i}_n \cdot \bar{i}_p)$.

The solenoidal velocity $\bar{U}_\psi$ is determined from an approximate vector potential calculation based upon the classical definition of vector potential (e.g., Newell [16]):

$$\bar{V} = \nabla \times \bar{\Psi} \ , \ \nabla \cdot \bar{\Psi} = 0 \ , \ \bar{\Omega} = \nabla \times \bar{V} = -\nabla^2 \bar{\Psi} \tag{10.2.9}$$

Here, it is assumed that $\bar{\Psi}$ is perpendicular to the transverse secondary flow planes and thus has the same direction as $\bar{i}_n$. Thus,

$$\bar{U}_\psi \equiv \nabla \times \psi_s \bar{i}_n \tag{10.2.10}$$

Consequently, $\bar{U}_\psi$ lies in the transverse secondary flow planes and

$$\xi_n = \bar{i}_n \cdot \bar{\Omega}_s = \bar{i}_n \cdot (\nabla \times \nabla \times \psi_s \bar{i}_n) \tag{10.2.11}$$

The function $\psi_s$ is analogous to a stream function defined in the transverse planes at each streamwise or axial location. Equation (10.2.11) is elliptic in the transvers planes and contains no streamwise derivatives, as a result of the assumption $\bar{\Psi} \doteq \psi_s \bar{i}_n$. Note that $\psi_s$ and thus $\bar{U}_\psi$ can be determined at each transverse plane from a knowledge of secondary vorticity $\xi_n$ in that plane, and no knowledge of $\xi_n$ at planes upstream or downstream is required, although $\xi_n$ itself depends upon upstream information.

The irrotational component $\bar{U}_\phi$ of the secondary flow velocity $\bar{U}_s$ is determined from the requirement that the overall velocity $\bar{U}$, including the viscous correction $\bar{U}_v$, satisfies local continuity. Actually, $\bar{U}_I$ and $\bar{U}_\psi$ satisfy continuity by construction, however as will be explained, $\bar{U}_v$ is determined from momentum considerations together with an integral continuity restraint, and consequently $\bar{U}_v$ does not necessarily satisfy local continuity. To ensure local continuity, $\bar{U}_\phi$ is determined such that

$$\nabla \cdot (\bar{U}_\phi + \bar{U}_v) = 0 \tag{10.2.12}$$

Furthermore, it is assumed that $\bar{U}_\phi$ lies in the transverse secondary flow planes and is derivable from a surface potential $\phi_s$ such that

$$\bar{U}_\phi \equiv \nabla\phi_s - \bar{i}_n(\bar{i}_n\cdot\nabla\phi_s) \tag{10.2.13}$$

Consequently, $\phi_s$ is governed by

$$\nabla^2\phi_s - \nabla\cdot\bar{i}_n(\bar{i}_n\cdot\nabla\phi_s) = -\nabla\cdot\bar{U}_v \tag{10.2.14}$$

which, given a knowledge of $\bar{U}_v$, is elliptic in the secondary flow planes.

Viscous Velocity Correction

The primary and secondary flow velocity components $\bar{U}_I$ and $\bar{U}_s$ satisfy slip conditions at solid boundaries. $\bar{U}_v$ corrects for the no-slip conditions, based on solution of an approximate momentum equation under the influence of "imposed" pressure gradients. The momentum equation is given by

$$(\bar{U}\ \nabla)\bar{U} + \frac{1}{\rho}\nabla p = \bar{F}(\bar{U}) \tag{10.2.15}$$

where $\bar{F}$ is the force due to viscous stress. Substituting decomposition formulas for velocity and pressure

$$\bar{U} = \bar{U}_I + \bar{U}_s + \bar{U}_v \quad , \quad p = p_I + p_s + p_v \tag{10.2.16}$$

there results

$$\left[(\bar{U}_I + \bar{U}_s + \bar{U}_v)\cdot\nabla\right](\bar{U}_I + \bar{U}_s + \bar{U}_v) + \frac{1}{\rho}\nabla(p_I + p_s + p_v) = \bar{F}(\bar{U}_I + \bar{U}_s + \bar{U}_v) \tag{10.2.17}$$

Borrowing a concept from boundary layer theory, it is assumed that the pressure gradients to be imposed are determined by $\bar{U}_I + \bar{U}_s$, which satisfy slip contiions. Thus,

$$\frac{1}{\rho}\nabla(p_I + p_s) = \bar{F}(\bar{U}_I + \bar{U}_s) - \left[(\bar{U}_I + \bar{U}_s)\cdot\nabla\right](\bar{U}_I + \bar{U}_s) \tag{10.2.18}$$

It should be noted that although $\bar{U}_s$ satisfies slip conditions, $\bar{U}_s$ and the resulting pressure gradients are not really "inviscid", since viscous terms are retained in the streamwise vorticity equation, and the irrotational contribution $\bar{U}_\phi$ depends

upon the viscous correction $\bar{U}_v$. Combining (10.2.17) and (10.2.18), an equation governing the viscous correction $\bar{U}_v$ is obtained:

$$\left[(\bar{U}_I + \bar{U}_s)\ \nabla\right]\bar{U}_v + \left[\bar{U}_v \cdot \nabla\right](\bar{U}_I + \bar{U}_s + \bar{U}_v) + \frac{1}{\rho}\nabla p_v = \bar{F}(\bar{U}_v) \qquad (10.2.19)$$

Further assumptions are necessary to permit solution of (10.2.19) by forward marching integration for subsonic flows. Streamwise diffusion in the direction normal to the secondary flow planes is neglected. In addition, for the primary flow direction, $p_v$ is taken to be a function only of distance $s_p$ in the primary flow direction. For external flows, $p_v$ is taken as zero in the absence of elliptic viscous-inviscid interaction. For internal flows, $p_v$ represents a mean viscous pressure drop determined by the requirement that the integral mass flow be conserved. The momentum equation for the primary flow direction becomes

$$\bar{i}_p \cdot \left\{\left[(\bar{U}_I + \bar{U}_s)\cdot\nabla\right]\bar{U}_v + \left[\bar{U}_v \cdot \nabla\right](\bar{U}_I + \bar{U}_s + \bar{U}_v) + \frac{1}{\rho}\nabla p_v(s_p) - \bar{F}'(\bar{U}_v)\right\} = 0 \qquad (10.2.20)$$

where $\bar{F}'$ does not include streamwise diffusion. The integral mass flux condition for internal flows with no mass addition is

$$\iint_A \bar{i}_p \cdot \rho\bar{U} = \text{constant} \qquad (10.2.21)$$

Assumptions for $p_v$ appropriate for the transverse components of the momentum equation are the topic of a continuing investigation. However, a very simple (although highly approximate) method for determining the transverse components of $\bar{U}_v$ can be devised from arguments based upon Johnston's [17] empirical observations of three-dimensional turbulent boundary layer velocity profiles having triangular polar diagrams. The triangular polar plots display a structure such that in the outer (inviscid) region, the skewing of the velocity is consistent with secondary flow theory, and in particular is related to the turning of the free stream in accordance with the Squire & Winter [3] secondary flow approximation. In the inner (viscous) region, the velocity profile is found to be collateral, such that v/u = constant. This suggests the following formula for computing the transverse components of $\bar{U}_v$:

$$\bar{U}_v = (\bar{U}_I + \bar{U}_s)\left[\frac{\bar{i}_p \cdot (\bar{U}_I + \bar{U}_s + \bar{U}_v)}{\bar{i}_p \cdot (\bar{U}_I + \bar{U}_s)} - 1\right] \qquad (10.2.22)$$

The formula (10.2.22) has the following properties: (1) in the outer portion of the viscous region, where $\bar{i}_p \cdot \bar{U}_V \to 0$, the composite velocity $\bar{U}$ reduces to $\bar{U}_I + \bar{U}_S$, (2) the composite velocity $\bar{U}$ satisfies the no-slip condition and is collateral near the wall. Improved approximations for the near-wall region are possible but are not considered here.

Energy Equation

Application of the present theory to nonadiabatic flows requires solution of the energy equation, which can be written

$$\nabla \cdot \rho \bar{U} E = \nabla \cdot \sigma \nabla T + \bar{U} \cdot \bar{F} + \Phi \tag{10.2.23}$$

Solution of (10.2.23) by forward marching integration requires only that $\bar{F}$ be replaced by $\bar{F}'$ and that terms representing the streamwise conduction of heat be neglected.

Compressibility Effects

The foregoing analysis has been formulated primarily for incompressible flows, for which the density $\rho$ is constant. For relatively small Mach numbers, however, compressibility effects can be represented in an approximate sense by introducing the perfect gas equation of state $p = \rho RT$ in the imposition of streamwise pressure gradients. Eliminating temperature T using the temperature-enthalpy relation

$$T = (\gamma - 1) M^2 \left( E - \frac{\bar{U} \cdot \bar{U}}{2} \right) \tag{10.2.24}$$

the following relation for representing streamwise pressure gradients is obtained:

$$\bar{i}_p \cdot \nabla (p_I + p_s + p_v) = \bar{i}_p \cdot \nabla \left[ \frac{\gamma - 1}{\gamma} \rho \left( E - \frac{\bar{U} \cdot \bar{U}}{2} \right) \right] \tag{10.2.25}$$

which provides an auxiliary equation relating density, velocity and total enthalpy. A slight modification results if $\bar{U} \cdot \bar{U}$ is replaced by $(\bar{i}_p \cdot \bar{U})^2$. A more comprehensive treatment of compressibility effects is possible but is not considered here.

## APPLICATION TO A CURVED FLOW PASSAGE

The general analysis of the previous sections is applied to the flow in a curved duct which is shaped like a turbine blade passage. A cross section of the duct geometry is shown in Fig. 1 and consists of two curved walls corresponding to the surfaces of turbine blades. The remaining boundaries of the flow passage are two parallel flat surfaces comprising the endwalls. In the particular case being considered, the geometry and inviscid flow are two-dimensional. However, the viscous flow is three-dimensional, particularly near the endwalls, where the transverse pressure gradients associated with the turning of the flow produce strong secondary flow toward the low pressure or suction surface side of the passage. A primary objective of this initial application is to demonstrate that the present analysis can predict endwall flows and the associated corner vortex region which are typical of that known to exist experimentally in geometries of this type.

### Coordinate System

Curvilinear orthogonal coordinates x, y, z are constructed to fit the flow passage boundaries as shown in Fig. 1. Metric coefficients $h_1$, $h_2$, $h_3$ are defined such that incremental distance $\delta s$ is determined by $(\delta s)^2 = (h_1\delta x)^2 + (h_2\delta y)^2 + (h_3\delta z)^2$. In planes parallel to the endwalls, orthogonal streamlines and velocity potential lines from a two-dimensional incompressible potential flow analysis are utilized as the coordinate lines for constant y and x, respectively. The z direction can be regarded as Cartesian, and thus $h_3 = 1$. The x coordinate is the primary flow or axial coordinate, and is associated with surfaces for which $\phi_I$ is constant. The y and z coordinates define transverse secondary flow planes at any given x location. In this coordinate system, the potential flow direction $\bar{i}_p$ and the normals $\bar{i}_n$ to the transverse planes coincide with $\bar{i}$, the unit vector in the x direction. A two-dimensional incompressible potential flow analysis and computer program developed by Anderson [18] was employed in the present investigation, without modification, to compute the necessary coordinate data and potential flow solution.

### Governing Equations

Throughout the remaining discussion, all variables in the governing equations are nondimensional, having been normalized by the following reference quantities: distance, $L_r$; velocity, $U_r$; density, $\rho_r$; temperature, $T_r$; total enthalpy, $U_r^2$;

pressure, $\rho_r U_r^2$; viscosity, $\mu_r$. Here the subscript r denotes a reference quantity. This normalization leads to the following nondimensional parameters: Mach number, M; Reynolds number, Re; Prandtl number, Pr; and specific heat ratio, $\gamma$. These parameters are defined by

$$M = U_r/c \ , \ Re = \rho_r U_r L_r/\mu_r \ , \ Pr = c_p \mu_r / k \ , \ \gamma = c_p / c_v \tag{10.3.1}$$

where $\mu_r$ is the molecular viscosity, k is thermal conductivity, and $c_p$ and $c_v$ are the specific heats at constant pressure and volume. The reference speed of sound, c, is defined by $c^2 = \gamma R_g T_r$, where $R_g$ is the gas constant.

Since in the present application the coordinate lines coincide with the potential flow streamlines and potential surfaces, the following simplifications hold: $v_I = w_I = u_s = 0$. The velocity decomposition (10.2.1) can thus be expressed as

$$\bar{U} = \bar{i}u + \bar{j}v + \bar{k}w = \bar{i}(u_I + u_v) + \bar{j}(v_s + v_v) + \bar{k}(w_s + w_v) \tag{10.3.2}$$

where $\bar{i}$, $\bar{j}$, $\bar{k}$ are unit vectors in the x, y, z coordinate directions, respectively. Under the stated assumptions, the streamwise vorticity equation can be written as

$$\frac{u_I}{Q}\left(u\frac{\partial \xi}{\partial x} - \xi\frac{\partial u}{\partial x}\right) + \frac{v_s}{Q}\frac{h_1}{h_2}\left(u\frac{\partial \xi}{\partial y} - \xi\frac{\partial u}{\partial y}\right) + \frac{w_s}{Q}h_1\left(u\frac{\partial \xi}{\partial z} - \xi\frac{\partial u}{\partial z}\right)$$
$$= -\frac{2}{h_2}\frac{\partial h_1}{\partial y}u\frac{\partial u}{\partial z} + \frac{\mu}{Re}\left(\frac{\partial}{\partial y}\frac{1}{h_1 h_2}\frac{\partial h_1 \xi}{\partial y} + h_1\frac{\partial^2 \xi}{\partial z^2}\right) \tag{10.3.3a}$$

where $Q^2 = u_I^2 + v_s^2 + w_s^2$, and the vorticity is related to velocity by

$$\xi_n = \xi = \frac{1}{h_2}\left(\frac{\partial w_s}{\partial y} - \frac{\partial h_2 v_s}{\partial z}\right) \tag{10.3.3b}$$

The secondary velocities are given by

$$v_s = \frac{1}{h_2}\frac{\partial \phi_s}{\partial y} + \frac{1}{h_1}\frac{\partial h_1 \psi_s}{\partial z} \tag{10.3.4a}$$

$$w_s = \frac{\partial \phi_s}{\partial z} - \frac{1}{h_1 h_2}\frac{\partial h_1 \psi_s}{\partial y} \tag{10.3.4b}$$

where the scalar and vector potential functions $\phi_s$ and $\psi_s$ are governed by

$$\frac{1}{h_2}\frac{\partial}{\partial y}\frac{1}{h_1 h_2}\frac{\partial}{\partial y}h_1\psi_s + \frac{1}{h_1}\frac{\partial^2 h_1\psi_s}{\partial z^2} = -\xi \tag{10.3.5}$$

and

$$\frac{\partial}{\partial y}\frac{h_1}{h_2}\frac{\partial\phi_s}{\partial y} + h_1 h_2\frac{\partial^2\phi_s}{\partial z^2} = -\left(\frac{\partial h_2 u_v}{\partial x} + \frac{\partial h_1 v_v}{\partial y} + \frac{\partial h_1 h_2 w_v}{\partial z}\right) \tag{10.3.6}$$

The streamwise momentum equation is approximated by

$$\begin{aligned}\frac{\partial}{\partial x}(h_2\rho u^2) + \left[\frac{\partial}{\partial y} + \frac{1}{h_1}\frac{\partial h_1}{\partial y}\right]h_1\rho u(v_s+v_v) + h_1 h_2\frac{\partial}{\partial z}\left[\rho u(w_s+w_v)\right]\\ -\rho(v_s+v_v)^2\frac{\partial h_2}{\partial x} + h_2\frac{\partial(p_I+p_s)}{\partial x} + h_2\frac{dp_v(x)}{dx}\\ = \frac{h_1}{Re}\frac{\partial}{\partial y}\frac{\mu}{h_2}\frac{\partial u}{\partial y} + \frac{h_1 h_2}{Re}\frac{\partial}{\partial z}\mu\frac{\partial u}{\partial z}\end{aligned} \tag{10.3.7}$$

The energy equation is approximated by

$$\begin{aligned}&\frac{\partial}{\partial x}(h_2\rho uE) + \frac{\partial}{\partial y}\left[h_1\rho(v_s+v_v)E\right] + \frac{\partial}{\partial z}\left[h_1 h_2\rho(w_s+w_v)E\right]\\ &= \frac{h_1}{Re}\frac{\partial}{\partial y}\left\{\frac{\mu}{Pr}\frac{1}{h_2}\frac{\partial E}{\partial y} + \frac{1}{2h_2}\left(\mu-\frac{\mu}{Pr}\right)\frac{\partial}{\partial y}\left[u^2+(w_s+w_v)^2\right]\right\}\\ &+ \frac{h_1 h_2}{Re}\frac{\partial}{\partial z}\left\{\frac{\mu}{Pr}\frac{\partial E}{\partial z} + \frac{1}{2}\left(\mu-\frac{\mu}{Pr}\right)\frac{\partial}{\partial z}\left[u^2+(v_s+v_v)^2\right]\right\}\end{aligned} \tag{10.3.8}$$

The imposed pressure gradients are determined from

$$h_2\frac{\partial(p_I+p_s)}{\partial x} = -\frac{\partial}{\partial x}(h_2 u_I^2) - \left[\frac{\partial}{\partial y} + \frac{1}{h_1}\frac{\partial h_1}{\partial y}\right]h_1 u_I v_s - h_1 h_2\frac{\partial}{\partial z}u_I w_s + v_s^2\frac{\partial h_2}{\partial x} \tag{10.3.9}$$

and related to the dependent variables using the following form of the auxiliary gas law relation (10.2.25)

$$\frac{\partial}{\partial x}\left[\frac{\gamma-1}{\gamma}\rho\left(E-\frac{u^2}{2}\right)\right] = \frac{\partial(p_I+p_s)}{\partial x} + \frac{dp_v(x)}{dx} \tag{10.3.10}$$

The integral mass flux relation is

$$\iint_A h_2 \rho u \, dy dz = \text{constant} \tag{10.3.11}$$

The collateral flow assumption (10.2.22) leads to the following equations for computing $v_v$, $w_v$:

$$v_v = v_s\left(\frac{u}{u_I} - 1\right) \tag{10.3.12a}$$

$$w_v = w_s\left(\frac{u}{u_I} - 1\right) \tag{10.3.12b}$$

Numerical Method

The governing equations are replaced by finite-difference approximations. Three-point central difference formulas are used for all transverse spatial derivatives. An analytical coordinate transformation devised by Roberts [19] is employed as a means of introducing a nonuniform grid in each transverse coordinate direction, to concentrate grid points in the wall boundary layer regions. Second-order accuracy for the transverse directions is rigorously maintained. Two-point backward difference approximations are generally used for streamwise derivatives, although this is not essential. The streamwise vorticity equation (10.3.3) is decoupled from other equations in the system and linearized with respect to $\xi$ by an ad hoc process consisting of lagging quantities not yet available at the implicit level. The resulting implicit difference equation for $\xi$ is solved using a scalar ADI scheme based on the technique of Douglas & Gunn [20] for generating ADI schemes as perturbations of fundamental implicit schemes. Equations (10.3.5 - 10.3.6) for the scalar and vector potential functions $\phi_s$ and $\psi_s$ are elliptic in the transverse planes and are solved, given values for the right-hand sides, using scalar iterative ADI. Specifically, the Douglas-Gunn perturbation of the Crank-Nicolson scheme is used. The streamwise momentum (10.3.7), energy (10.3.8) and auxiliary gas law relation

(10.3.10) are solved as a coupled system using linearized block ADI. A detailed discussion of the block ADI scheme used has been given by McDonald & Briley [21] and Briley & McDonald [22]. The general approach is to linearize the implicit equations by formal expansion about the solution at the most recent axial location. Terms in the difference equations are then grouped by coordinate direction, and the Douglas-Gunn [20] technique is used to generate an ADI scheme. The resulting difference equations can be written in block-tridiagonal or a closely related matrix form and solved efficiently by block elimination techniques.

A summary of the overall algorithm used to advance the solution a single axial step follows. It is assumed that the solution is known at the n level $x^n$ and is desired at $x^{n+1}$.

(1) The streamwise vorticity equation (10.3.3) is solved using scalar ADI to obtain $\xi^{n+1}$.

(2) The vector potential equation (10.3.5) is solved using scalar iterative ADI to obtain $\psi_s^{n+1}$.

(3) Values for $v_s$ and $w_s$ are computed using equation (10.3.4). Values of $\phi_s^n$ obtained from the previous step are used. Values for $v_v$ and $w_w$ are computed from equations (10.3.12). The imposed pressure gradients $\partial(p_I + p_s)/\partial x$ are computed from equation (10.3.9).

(4) A value for the mean viscous pressure drop $dp_v(x)/dx$ is assumed. Initially, the value from the previous step is used.

(5) Equations (10.3.7), (10.3.8), & (10.3.10) are solved as a coupled system using block ADI to obtain values of $u^{n+1}$, $\rho^{n+1}$ and $E^{n+1}$. In general, the integral mass flux relation (10.3.11) will not be satisfied.

(6) Return to step (4) and repeat this process iteratively using the standard secant method [23] to find the value of the mean viscous pressure drop which leads to $u^{n+1}$ and $\rho^{n+1}$ which satisfies the integral mass flux relation (10.3.11). The secant method was found in practice to converge to five figures on the third iteration.

(7) Using values now available for $\partial u/\partial x$, the scalar potential equation (10.3.6) is solved using scalar iterative ADI to obtain $\phi_s^{n+1}$ for use in the next axial step.

To start this procedure, values for $\phi^n$ are needed. These are obtained by solving steps (4-7) above, under the assumption that the transverse velocity components are zero.

Computed Solution

A sample laminar flow calculation was performed, to evaluate the overall method in its present state of development and thus explore the potential of the present method for making detailed predictions of the flow and heat transfer in turbine blade passages. The solution was computed for the geometry of Fig. 1, and the Reynolds number based on the duct width at the inlet was 1000. The ratio of the distance between endwalls to the distance between blade surfaces at the passage entrance was 3.08. Blade boundary layers at the upstream starting plane were assumed to have a thickness of 0.05 times the distance between blade surfaces. The endwall boundary layer was taken to be twice this thickness. Adiabatic walls were assumed, and the following flow parameters were used: Mach number $M = 0.1$, Prandtl number $Pr = 1.0$, specific heat ratio $\gamma = 1.4$. A 20 x 20 grid was used for the cross section, and 24 axial steps were computed.

The ability of the present analysis to predict the formation and development of a corner vortex is of primary interest here. The existence of a corner vortex for this type of flow problem has been established for some time (e.g., Herzig, Hansen & Costello [24]). The flow structure consists of a strong secondary flow near the endwall and toward the low pressure or suction surface, caused by transverse pressure gradients associated with the turning of the primary flow. Upon reaching the suction surface, the secondary flow proceeds up the suction surface a short distance and then back into the primary flow, forming a streamwise vortex in the corner formed by the intersection of the suction surface and the endwall. Recently, more detailed experimental measurements and observations have been reported by Langston, Nice & Hooper [25] and Sjolander [26]. The authors are unaware of any previous numerical calculation which correctly predicts the formation and subsequent development of the corner vortex flow.

Computed streamlines very near the suction surface ("unwrapped" to lie in a plane) and near the endwall are shown in Fig. 2. These limiting streamlines provide a clear indication of the strong secondary flow near the endwall toward the suction surface and of the formation of the corner vortex (cf., [25], [26]). Additional computed results are included here in the form of contour plots of the u, v, and w components of velocity (relative to the potential flow direction) and of streamwise vorticity in transverse planes at selected streamwise locations. The location of the transverse planes, identified by axial step number, is shown in Fig. 3. Maximum and minimum contour values are given in Table I. Velocity contours at station 2 are shown in Fig. 4. This streamwise location is just

downstream of the initial plane, and thus little flow development has taken place. The secondary flow proceeds into the endwall boundary layer at the pressure surface, toward the suction surface, and out of the endwall boundary layer, but the velocities are of small magnitude. At station 12 in Fig. 5, strong crossflow in the endwall region and up the suction surface is quite apparent, and crossflow velocities on the order of 40% of the maximum streamwise velocity are present. The streamwise velocity contours have become distorted due to the corner vortex. At station 24 in Fig. 6, the corner vortex fills most of the lower part of the passage, and there is considerable distortion of the primary flow. A sequence of contour plots of streamwise vorticity $\xi$ is shown in Fig. 7. These contours also clearly show the formation and development of the corner vortex.

Finally, although computed results for the static and total pressure are ultimately of considerable interest, these are not included here since the results were found to contain anomalies which reflect the incomplete state of development of the computational algorithm and computer program at the time the test case was run. Subsequent detailed examination of the results has led to the belief that a straightforward refinement of the computational procedure will lead to considerable improvement in the predictions for pressure. Although not major, due to the time scales involved it was not possible to develop, implement and evaluate the needed changes within the constraints of the present study. Despite the inaccurate prediction of pressure, however, the analysis in its present state of development provided reasonable results for the secondary flow and corner vortex, and appears very promising as a tool for making detailed predictions of endwall flow and heat transfer.

## REFERENCES


1. Dodge, P.R.: A Numerical Method for 2-D and 3-D Viscous Flows. AIAA Paper No. 76-425, 1976.

2. Pratap, V.S. and D.B. Spalding: Fluid Flow and Heat Transfer in Three-Dimensional Duct Flows. Int. J. Heat & Mass Transfer, Vol. 19, 1976, p. 1183.

3. Squire, H.B. and K.G. Winter: The Secondary Flow in a Cascade of Airfoils in a Non-Uniform Stream. J. Aero. Sci., Vol. 18, 1951, p. 271.

4. Hawthorne, W.R.: The Applicability of Secondary Flow Analyses to the Solution of Internal Flow Problems. Fluid Mechanics of Internal Flow, Gino Sovran, Ed.; Elsevier Publishing Co., New York, New York, 1967.

5. Horlock, J.H. and B. Lakshminarayana: Secondary Flow; Theory, Experiment and Application in Turbomachinery Aerodynamics. Annual Reviews in Fluid Mechanics, Vol. 5, 1973, p. 247.

6. Lakshminarayana, B. and J.H Horlock: Generalized Expressions for Secondary Vorticity Using Intrinsic Coordinates. J. Fluid Mech., Vol. 59, 1973, p. 97.

7. Stuart, A.R. and R. Hetherington: The Solution of the Three Variable Duct Flow Equations. Fluid Mechanics, Acoustics and Design of Turbomachinery, NASA SP-304, 1974, pp. 135-154.

8. Nash, J.F. and V.C. Patel: Three-dimensional Turbulent Boundary Layers, SBC Technical Books, Atlanta, 1972.

9. Patankar, S.V. and D.B. Spalding: A Calculation Procedure for Heat, Mass, and Momentum Transfer in Three-dimensional Parabolic Flows. Int. J. Heat and Mass Transfer, Vol. 15, 1972, p. 1787.

10. Caretto, L.S., R.M. Curr and D.B. Spalding: Two Numerical Methods for Three-Dimensional Boundary Layers. Computational Methods in Applied Mechanics and Engineering, Vol. 1, 1973, p. 39.

11. Briley, W.R.: Numerical Method for Predicting Three-dimensional Steady Viscous Flow in Ducts. Journal of Computational Physics, Vol. 14, 1974, p. 8.

12. Ghia, K.N., V. Ghia and C.J. Studerus: Analytical Formulation of Three-dimensional Laminar Viscous Flow Through Turbine Cascades Using Surface-Oriented Coordinates. ASME Paper No. 76-FE-22, 1976.

13. Rubin, S.G. and P.K. Khosla: Laminar Flow in Rectangular Channels, Part II - Numerical Solution for a Square Channel. Computer Methods in Fluid Mechanics, ASME, 1976, p. 29.

14. Patankar, S.V., V.S. Pratap and D.B. Spalding: Prediction of Laminar Flow and Heat Transfer in Helically Coiled Pipes. Journal of Fluid Mechanics, Vol. 62, 1974, p. 539.

15. Ghia, K.N. and J.S. Sokhey: Laminar Incompressible Viscous Flow in Curved Ducts of Rectangular Cross-Sections. J. Fluids Engineering, Vol. 99, 1977, p. 640.

16. Newell, A.E.: Vector Analysis. McGraw-Hill, New York, 1955, p. 116.

17. Johnston, J.P.: On the Three-Dimensional Turbulent Boundary Layer Generated by Secondary Flow. J. Basic Engineering, Vol. 82, 1960, p. 233.

18. Anderson, O.L.: User's Manual for a Finite-Difference Calculation of Turbulent Swirling Compressible Flow in Axisymmetric Ducts with Struts and Slot Cooled Walls. USAAMRDL-TR-74-50, Vol. I., 1974.

19. Roberts, G.O.: Computational Meshes for Boundary Layer Problems. Proceedings of the Second International Conference on Numerical Methods in Fluid Dynamics. Springer-Verlag, New York, 1971, p. 171.

20. Douglas, J. and J.E. Gunn: A General Formulation of Alternating Direction Methods, Part I. Parabolic and Hyperbolic Problems. Numerische Mathematik, Vol. 6, 1964, p. 428.

21. McDonald, H. and W.R. Briley: Three-dimensional Supersonic Flow of a Viscous or Inviscid Gas. Journal of Computational Physics, Vol. 19, No. 2, 1975, p. 150.

22. Briley, W.R. and H. McDonald: Solution of the Multidimensional Compressible Navier-Stokes Equations by a Generalized Implicit Method. J. Comp. Phys., Vol. 24, 1977, p. 372.

23. Ralston, A.: A First Course in Numerical Analysis. McGraw-Hill, New York, 1965, p. 323.

24. Herzig, H.Z., A.G. Hansen and G.R. Costello: A Visualization Study of Secondary Flows in Cascades. NACA Report 1163, 1953.

25. Langston, L.S., M.L. Nice and R.M. Hooper: Three-dimensional Flow within a Turbine Cascade Passage. ASME Paper 76-GT-50, 1976.

26. Sjolander, S.A.: The Endwall Boundary Layer in an Annular Cascade of Turbine Nozzle Guide Vanes. Technical Report No. ME/A 75-4, Department of Mechanical and Aeronautical Engineering, Carleton University, Ottawa, Canada, 1975.

CASCADE GEOMETRY AND
COMPUTED COORDINATE SYSTEM

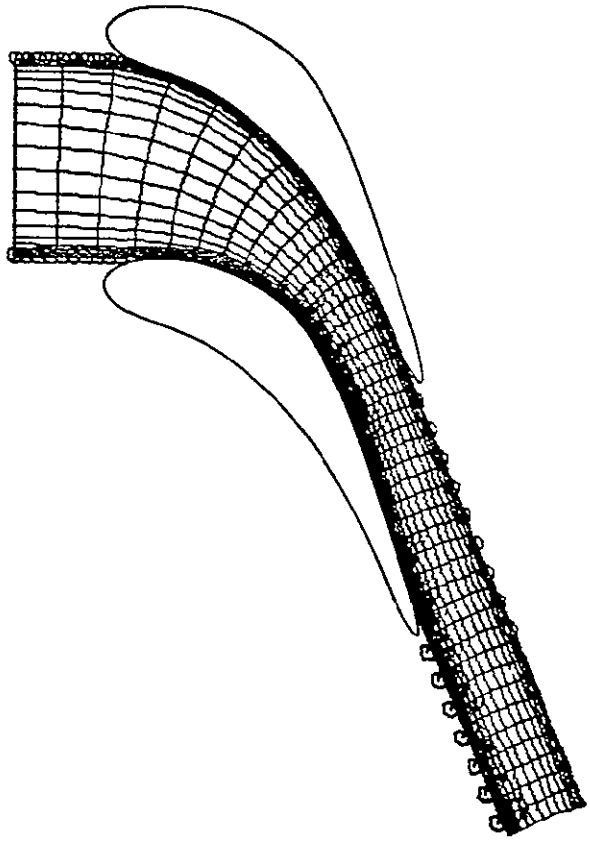

COMPUTED LIMITING STREAMLINES

(a) Endwall Surface

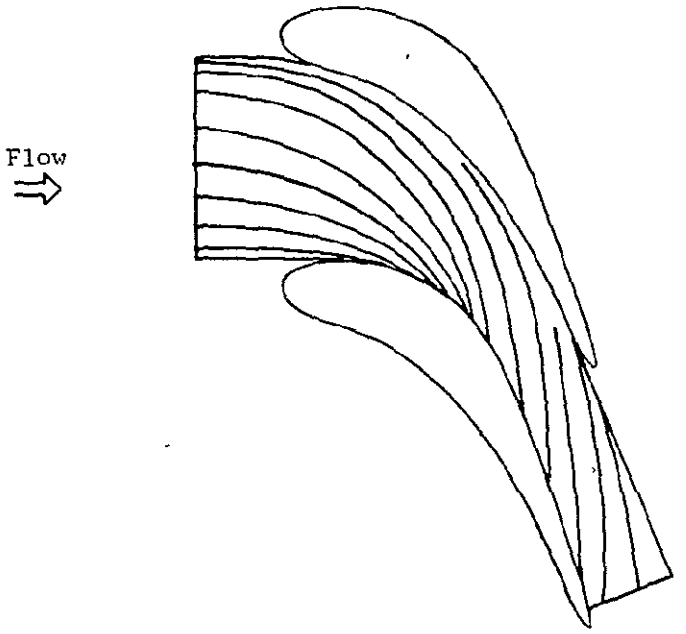


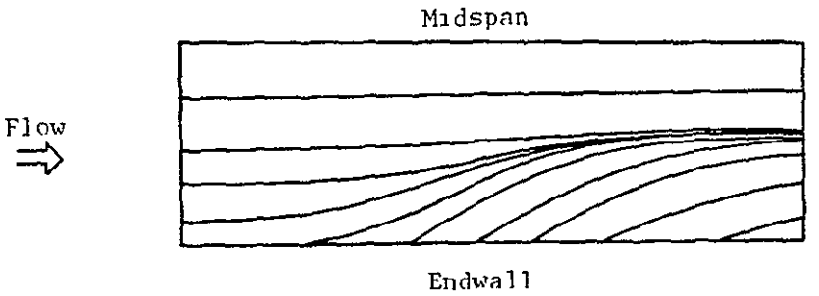


(b) Airfoil Suction Surface

LOCATION OF TRANSVERSE PLANES
AT SELECTED STREAMWISE LOCATIONS

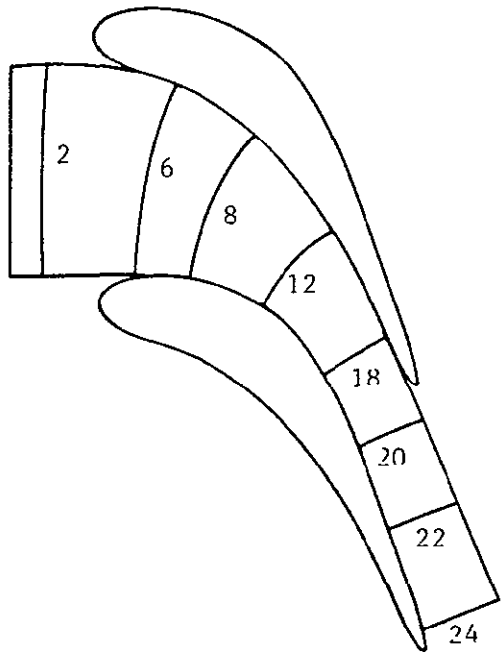

TABLE I - MAXIMUM AND MINIMUM CONTOUR VALUES
(OTHER CONTOURS ARE LINEARLY SPACED)

| Station | $u_{min}$ | $u_{max}$ | $v_{min}$ | $v_{max}$ | $w_{min}$ | $w_{max}$ | $\xi_{min}$ | $\xi_{max}$ |
|---|---|---|---|---|---|---|---|---|
| 2 | 0.0 | 0.96 | -0.034 | 0.014 | -0.008 | 0.011 | - 7.7 | - 0.77 |
| 6 | 0.0 | 1.34 | -0.19 | 0.04 | -0.08 | 0.15 | - 30.6 | - 2.9 |
| 8 | 0.0 | 1.77 | -0.41 | 0.08 | -0.11 | 0.48 | - 59.4 | - 5.7 |
| 12 | 0.0 | 2.25 | -0.87 | 0.11 | -0.21 | 0.66 | -129.0 | -12.7 |
| 18 | 0.0 | 2.81 | -0.76 | 0.13 | -0.29 | 0.86 | -186.0 | -18.4 |
| 20 | 0.0 | 2.79 | -0.58 | 0.13 | -0.32 | 0.69 | -158.0 | -15.7 |
| 22 | 0.0 | 2.71 | -0.45 | 0.14 | -0.33 | 0.61 | -124.0 | -12.4 |
| 24 | 0.0 | 2.62 | -0.36 | 0.16 | -0.34 | 0.52 | - 90.1 | - 4.65 |

CONTOURS OF STREAMWISE VELOCITY, u

Station 2

Pressure Surface

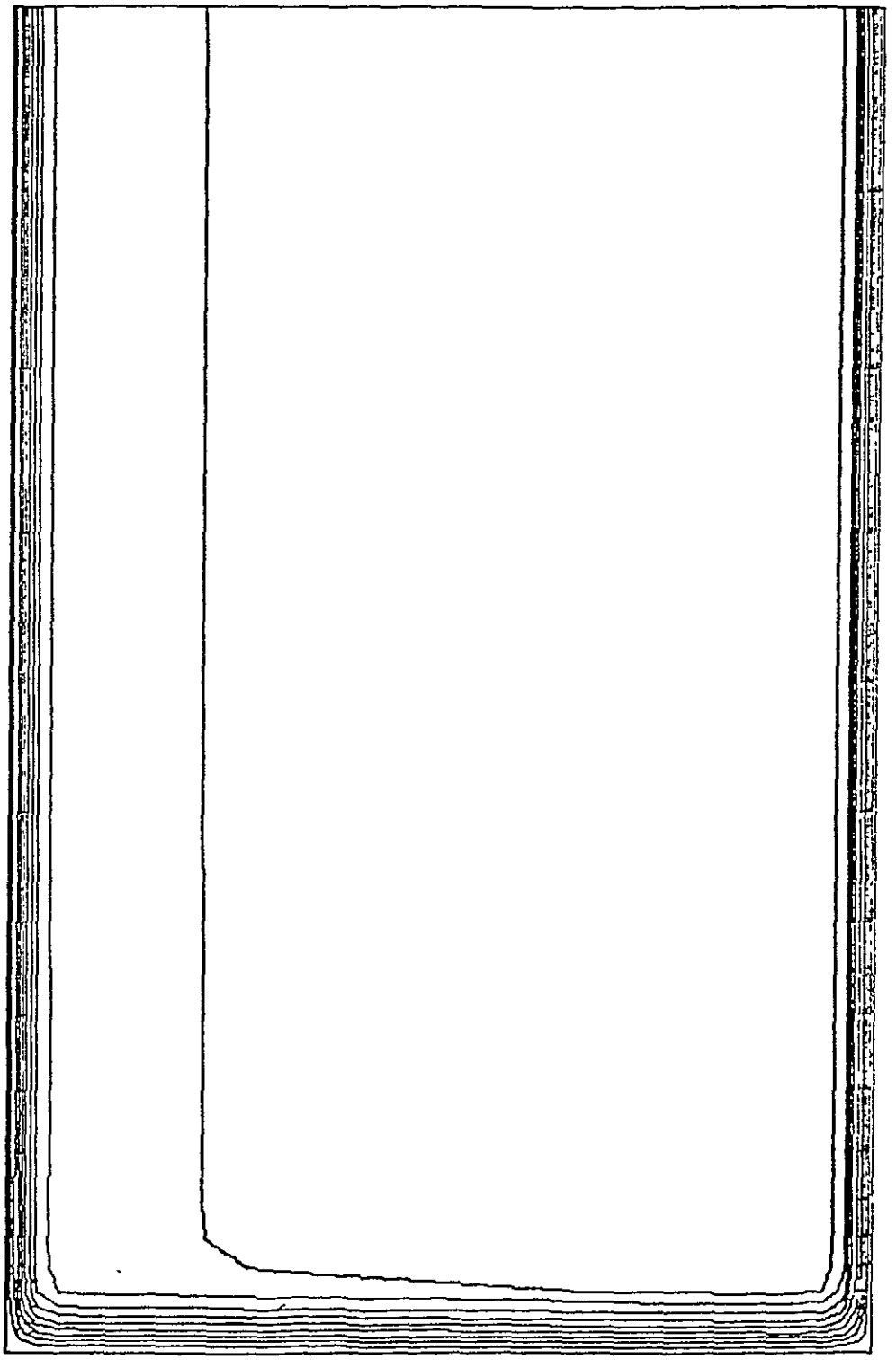

Suction Surface

Endwall

CONTOURS OF TRANSVERSE VELOCITY, v

Station 2

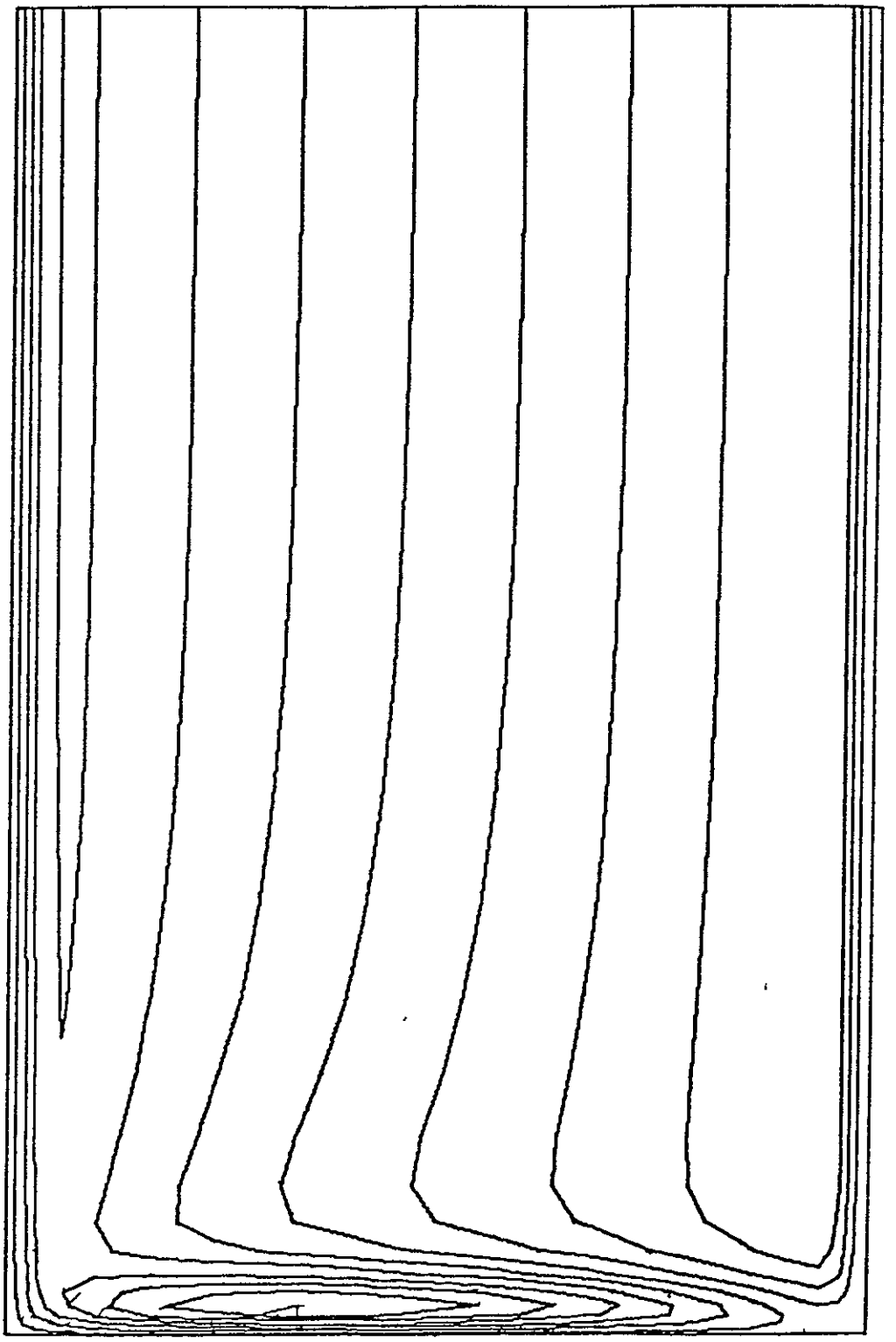

CONTOURS OF SPANWISE VELOCITY, w

Station 2

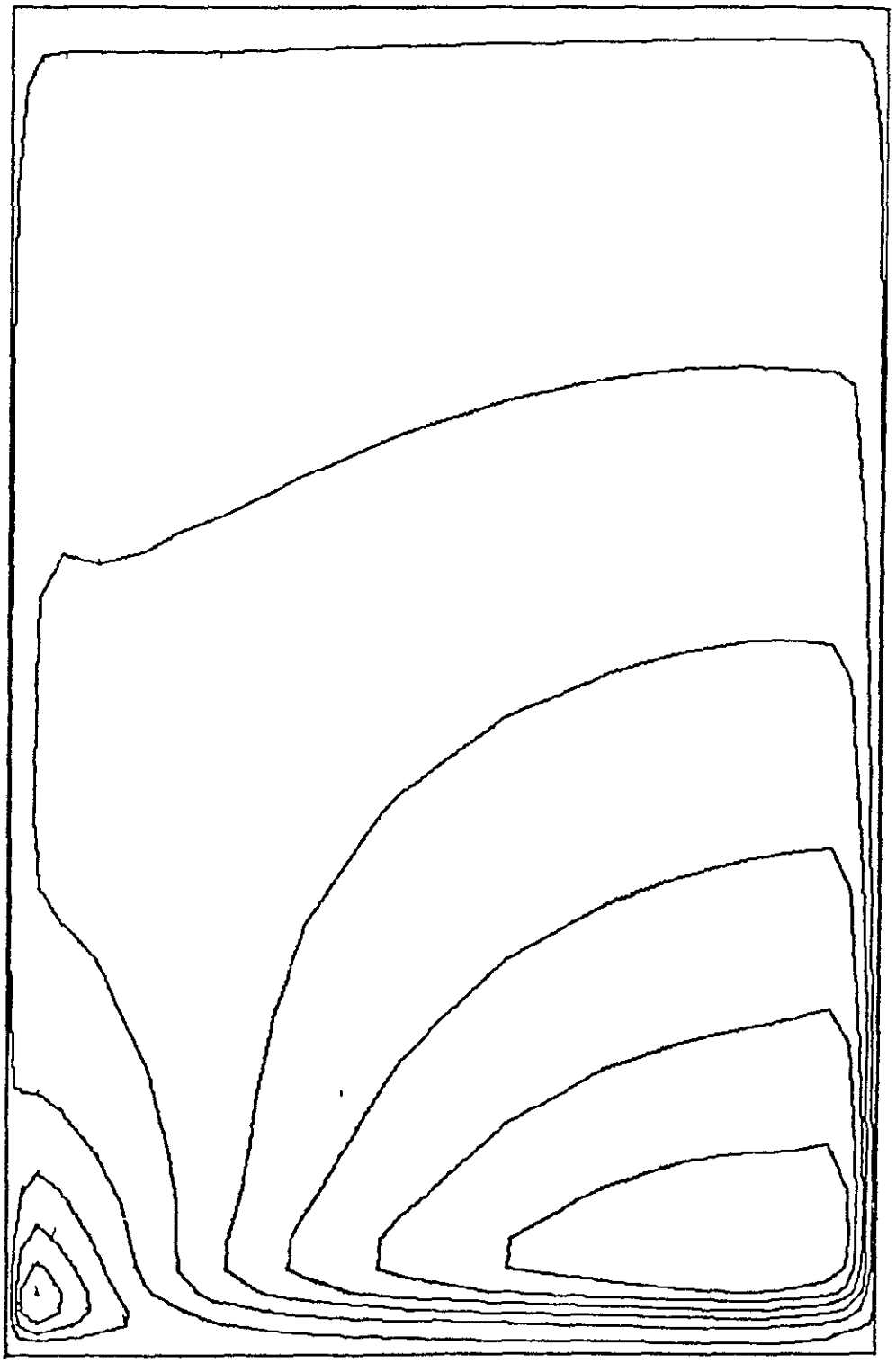

CONTOURS OF STREAMWISE VELOCITY, u

Station 12

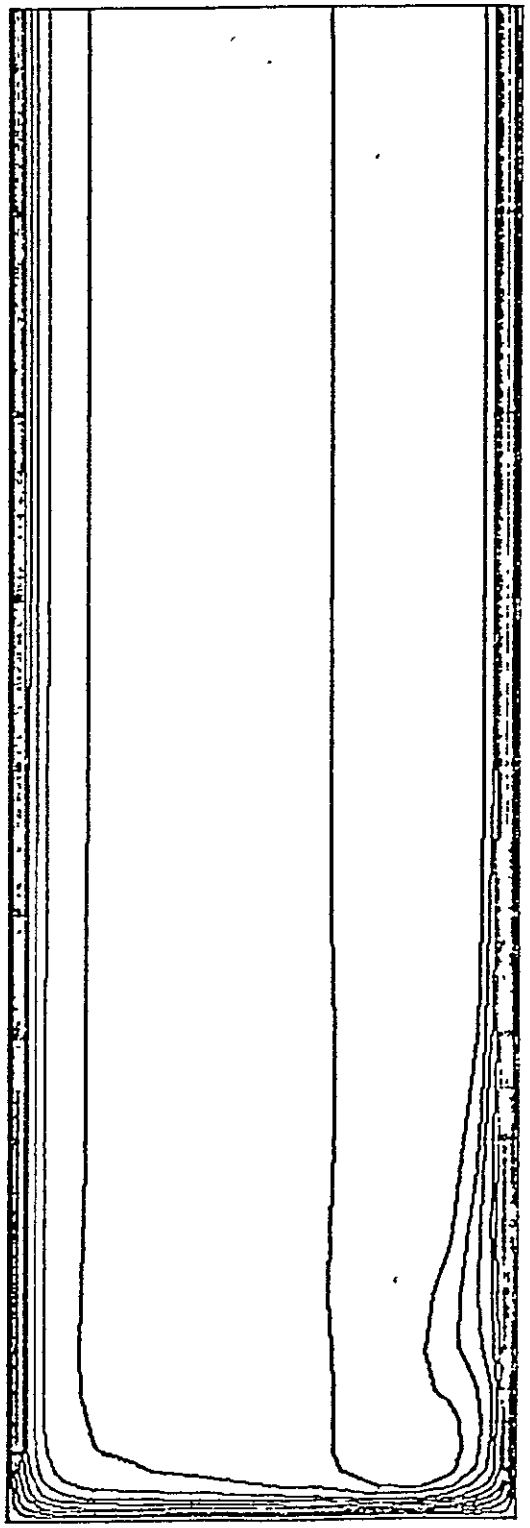

CONTOURS OF VELOCITY

Station 12

v - Component

w - Component

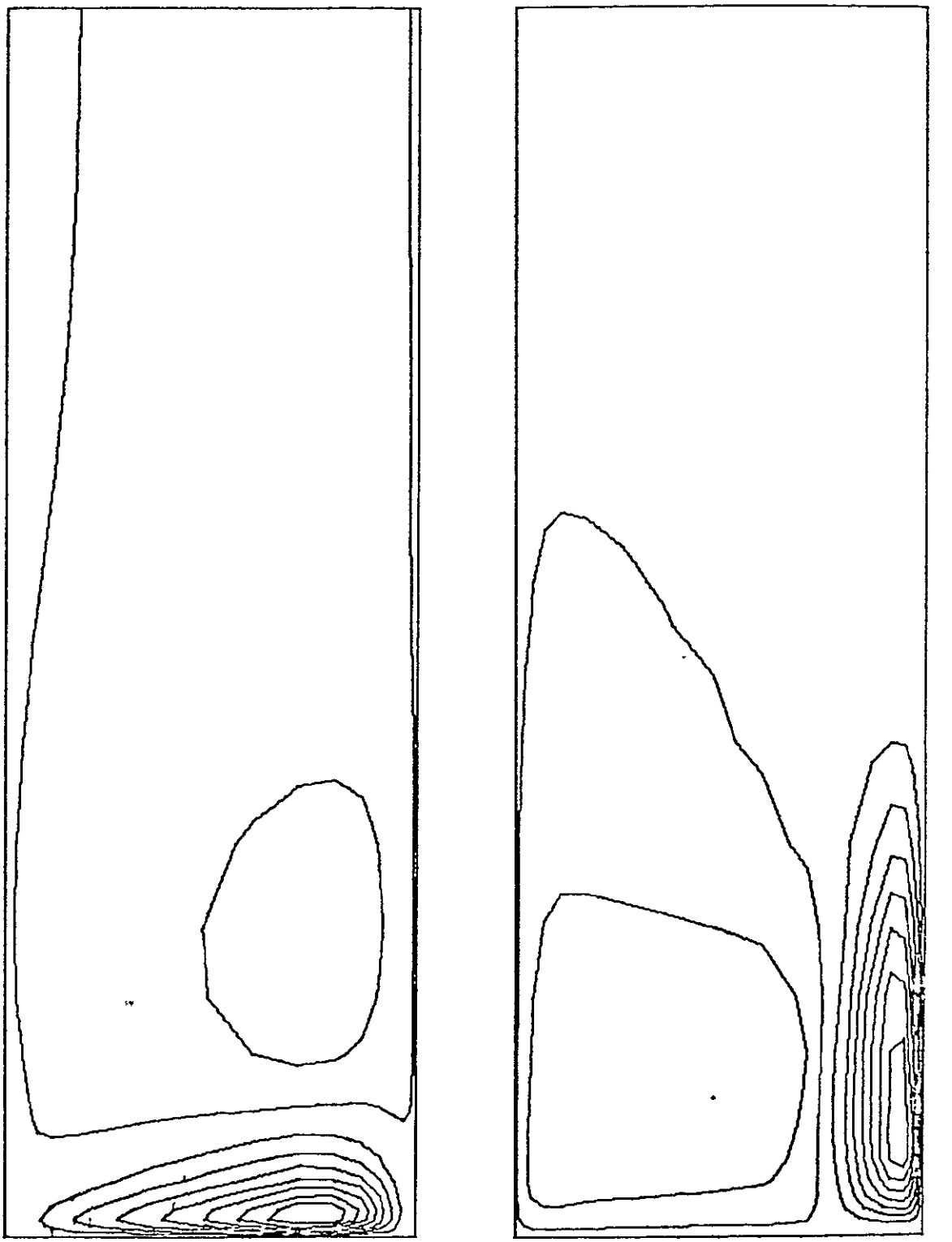

CONTOURS OF VELOCITY

Station 24

u - Component

v - Component

w - Component

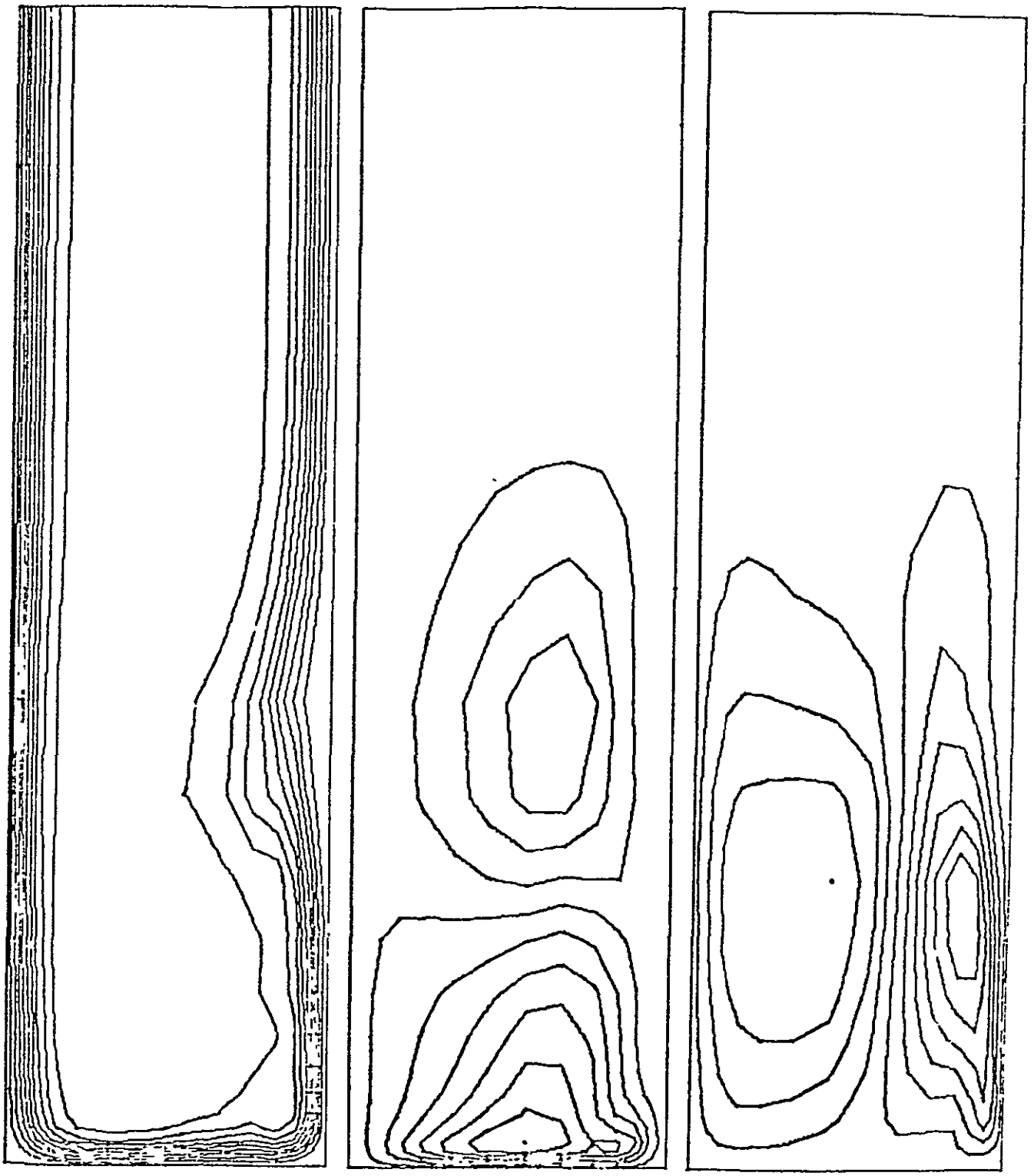

CONTOURS OF STREAMWISE VORTICITY, $\xi$

Station 2



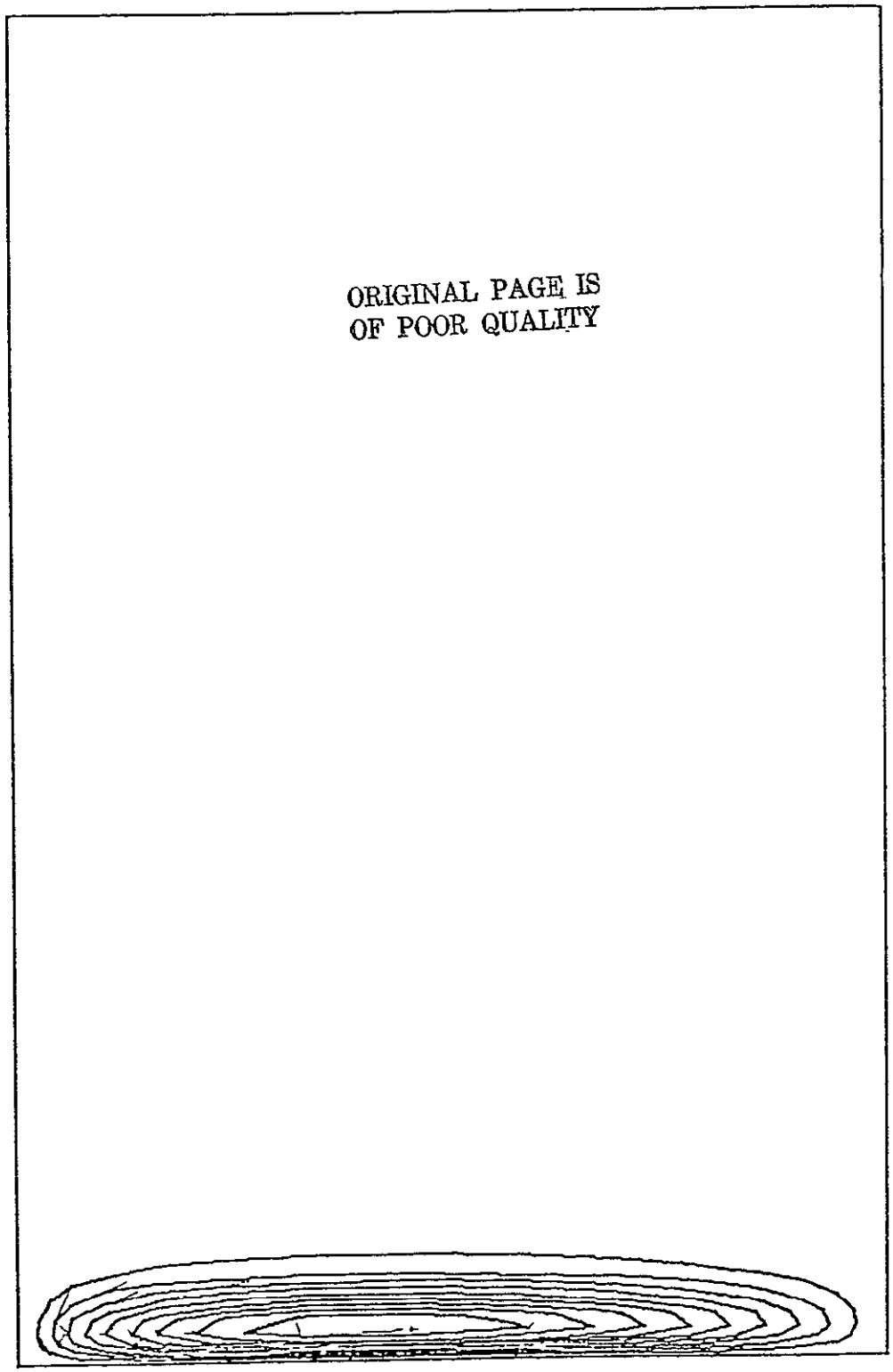

Pressure Surface

Suction Surface

Endwall

CONTOURS OF STREAMWISE VORTICITY, $\xi$

Station 6

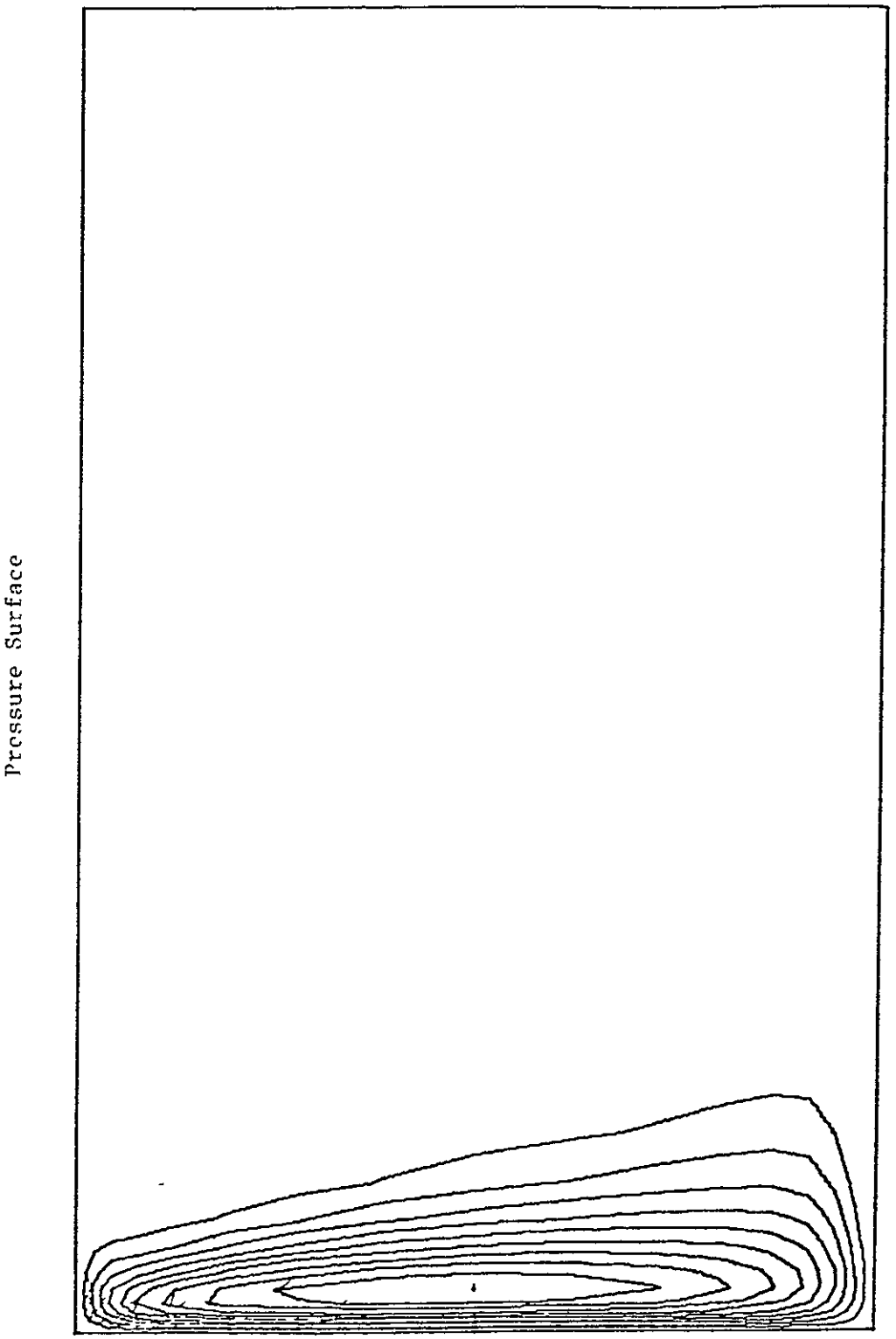

CONTOURS OF STREAMWISE VORTICITY, $\xi$



Station 8

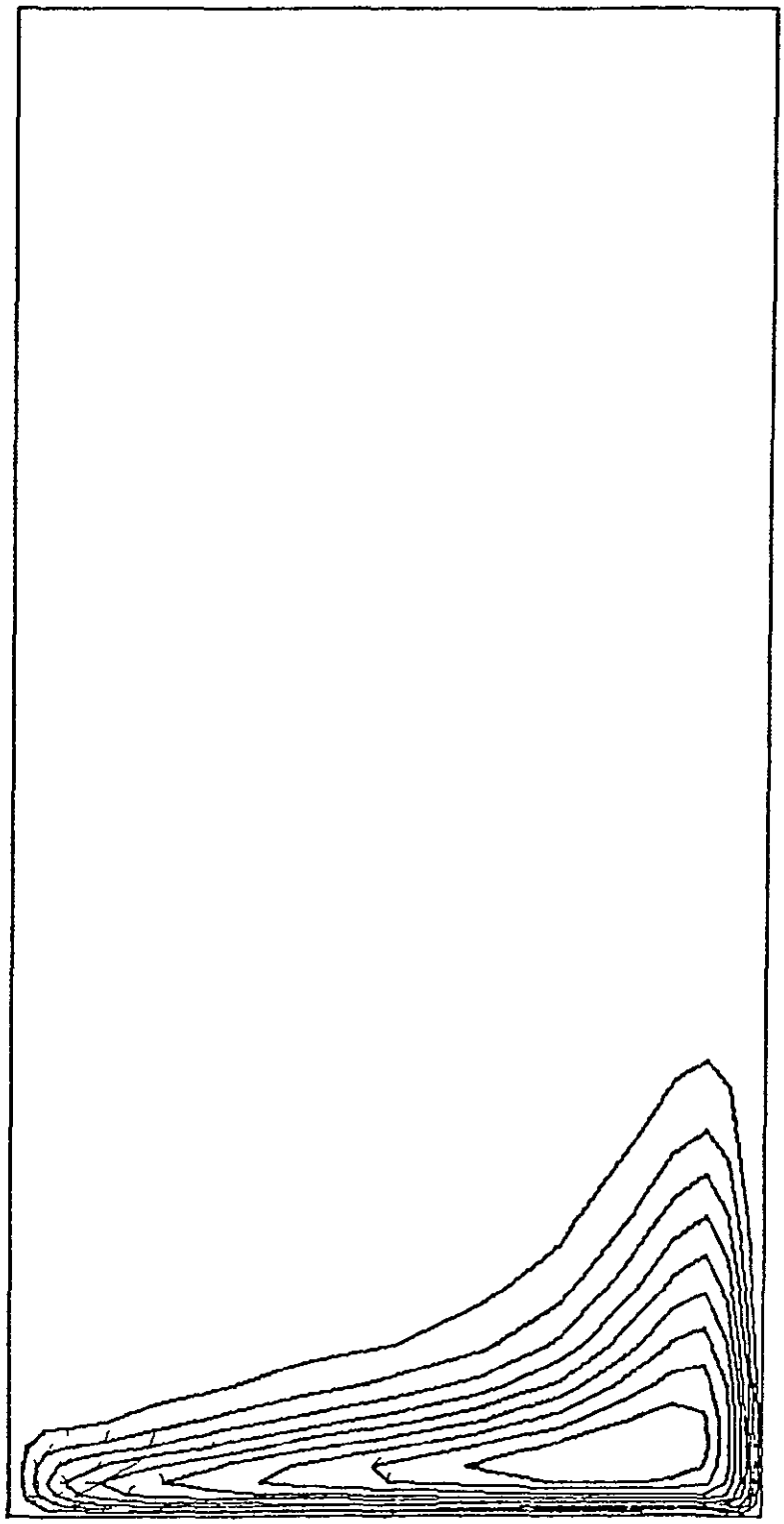

CONTOURS OF STREAMWISE VORTICITY, $\xi$

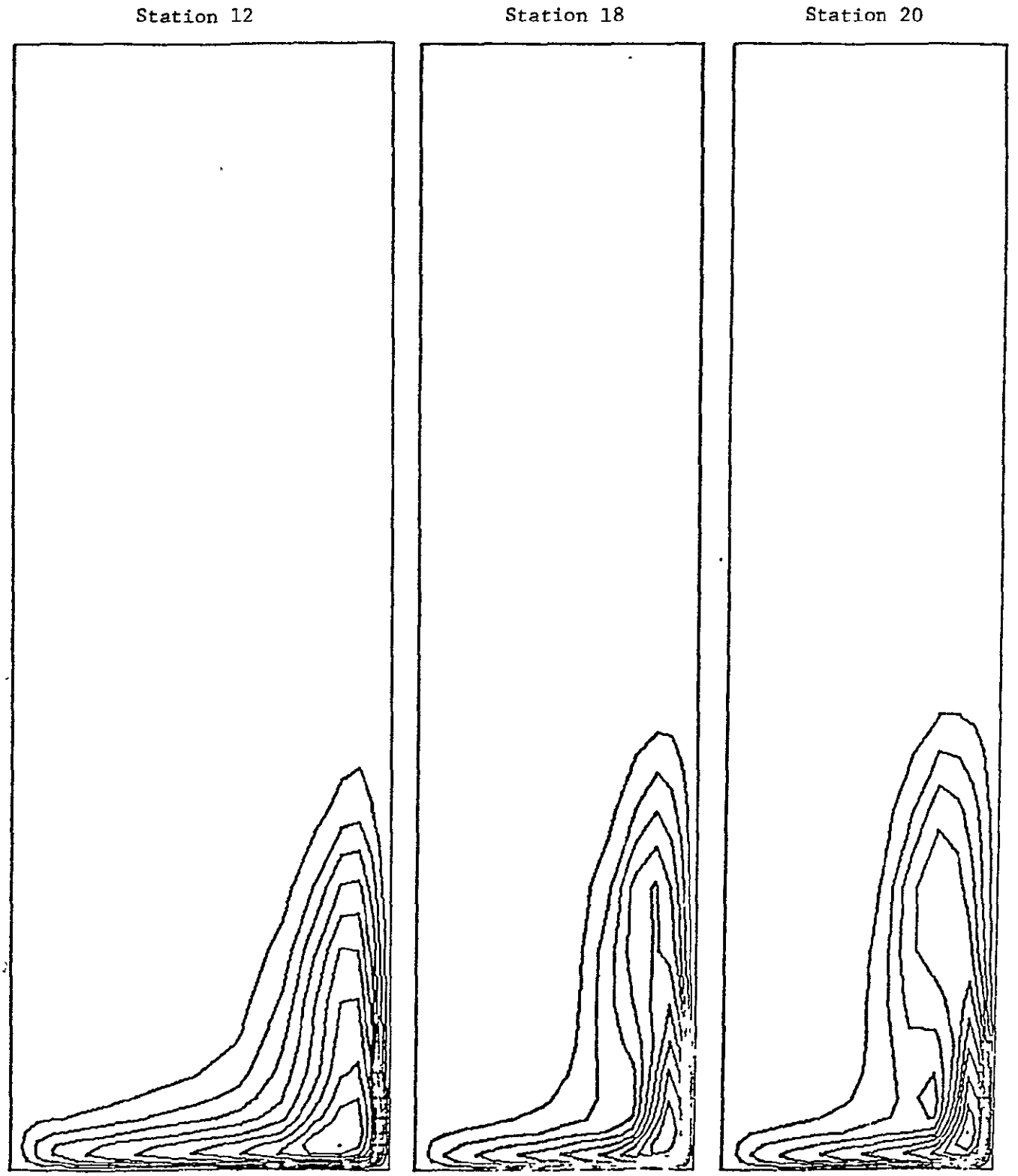

CONTOURS OF STREAMWISE VORTICITY, $\xi$



Station 22

Station 24

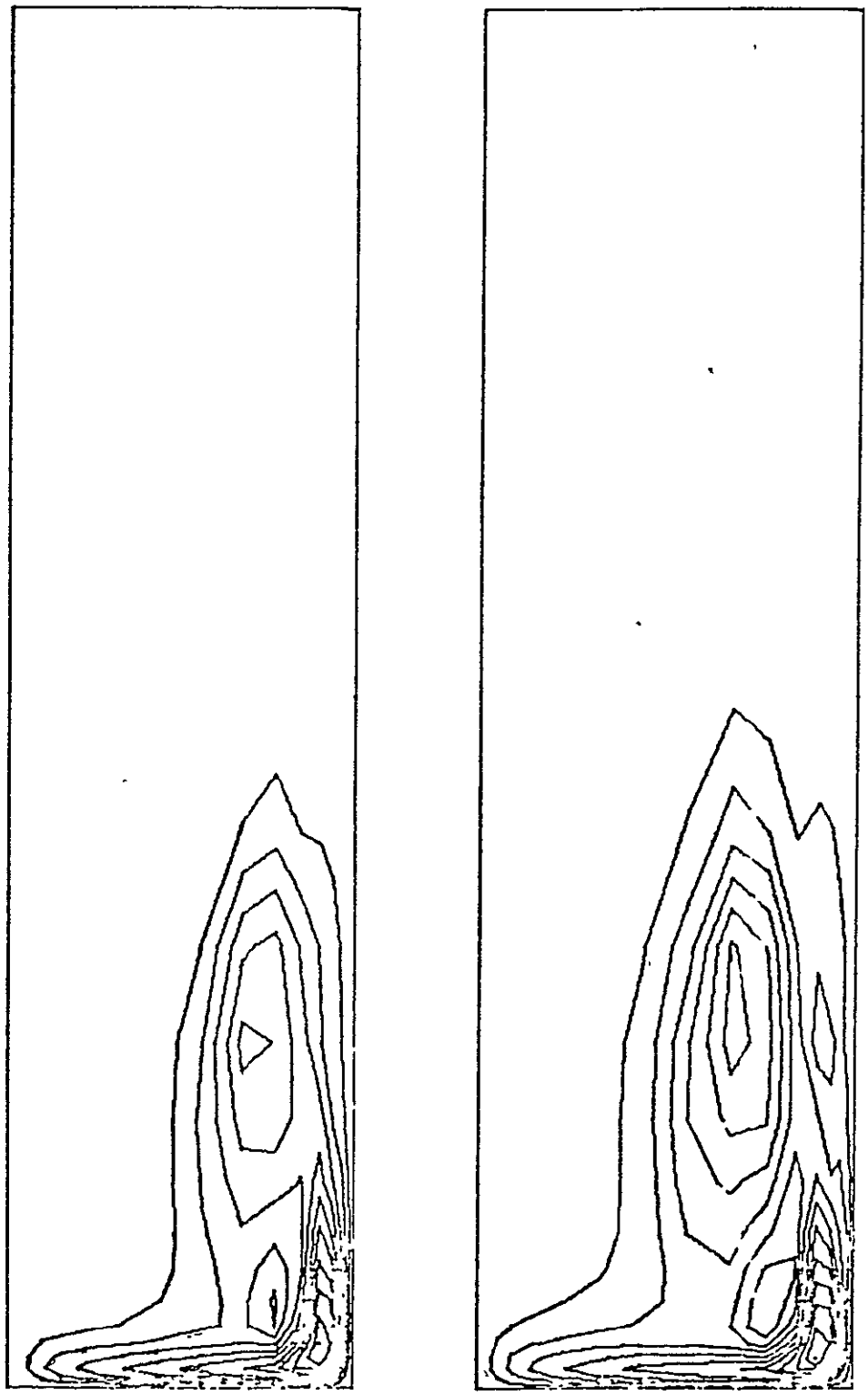

Pressure Surface

Suction Surface

Endwall

Endwall

# 11.0 DETAILED PROGRAM DESCRIPTIONS

## 11.1 MAIN PROGRAM GCCOOR

Object  Compute Coordinates of Circular Arc Duct

Options  IDBG6 = 0 Do not print coordinates

= 1 Print coordinates

NDRUM  2 Store coordinates on UNIT NDRUM

Input Symbols

DUCTI(1) = $d_1$ , Duct axial length (ft) (calculated)
DUCTI(2) = $d_2$ , Duct OD radius (ft)
DUCTI(3) = $d_3$ , Duct ID radius (ft)
DUCTI(4) = $d_4$ , Axial location of origin (ft)
DUCTI(5) = $d_5$ , Radial location of origin (ft)
DUCTI(6) = $d_6$ , Inlet angle (degrees)
DUCTI(7) = $d_7$ , Exit angle (degrees)
DUCTI(8) = $d_8$ , not used

TITLE(I) , Title 72 holarith characters
JL , Number of streamwise stations
KL , Number of streamlines
KDS = 1 ,
IDBG6 , Print option
NDRUM , Drum option
DDS , Mesh distortion parameter

Output Symbols

D1 = $\varepsilon$ , Roberts Transformation Parameter
USCALE = Vr , Metric scale factor
R(1,1,J) = $Y_{ID}$, R(1,4,J) = $X_{ID}$ } Coordinates of ID radius
R(2,1,J) = $Y_{OD}$, R(2,4,J) = $X_{OD}$ } Coordinates of OD radius
JSTEP , Streamwise station number

Theory

The coordinates for a circular arc duct can be obtained from the solution for a vortex flow. If W is the complex potential and Z the complex coordinate, we have

$$W = -i/n(z-z_o) = s + in \tag{1}$$

where $Z_o$ is the origin of the circular arc duct and S and n the potential flow coordinates. Let

$$R = [x-x_o)^2 + (Y-Y_o)^2]^{1/2} \tag{2}$$

$$\theta = \tan^{-1}[(Y-Y_o)/(X-X_o)] \tag{3}$$

Hence from (1) we have

$$S = \theta \tag{4}$$

$$n = -\ln R \tag{5}$$

The potential flow velocity (metric scale coefficient) is given by

$$\frac{1}{n} = v = \left|\frac{dW}{dz}\right| = \frac{1}{R} \tag{6}$$

The coordinate functions are then scaled such that

$$0 \leq n \leq 1 \tag{7}$$

Hence

$$n = \ln(R/R_{OD})/\ln(R_{ID}/R_{OD}) \tag{8}$$

$$S = R_{OD}/(R_{OD} - R_{ID})\cdot(\theta-\theta_o) \tag{9}$$

$$V = -\frac{1}{\ln(R_{ID}/R_{OD})}\,\frac{1}{R} \tag{10}$$

## 11.2 MAIN PROGRAM GDCOOR

Object — Compute coordinates of Arbitrary Duct

Options

IDBG6 = 0 Do not print coordinates
= 1 Print coordinates

NDRUM , Store coordinates on unit NDRUM

Input Symbols

| | | |
|---|---|---|
| JL | | , No. streamwise stations |
| KL | | , No. streamlines |
| KDS | = 1 | , No. steps/station |
| JLPTS | | , No. input data points |
| IDBG6 | | , Print option |
| NDRUM | | , Drum option |
| LFILE | | , = 0 do not use |
| DDS | | , Mesh distortion parameter |
| DUCTI(1) | $d_1$ | , Duct length (ft) |
| DUCTI(2) | $d_2$ | , No. knots |
| RD1I(J) | | , Input OD radius (ft) |
| RD2I(J) | | , Input ID radius (ft) |

Output Symbols

| | | |
|---|---|---|
| USCALE | $U_s$ | , Metric normalizing factor |
| EPS | $\epsilon$ | , Roberts Transformation Parameter |

(See Ref. 12 for complete list)

Theory

The input data points are smoothed by using a least squares spline fit of the second derivative with $d_2$ knots. This smoothed second derivative is then integrated to get the smooth contour. The duct coordinates are obtained using the conformal mapping procedure described in Ref. 18.